1988

Development of a two-dimensional finite element soil-moisture flow model

Mushtaque Ahmed
Iowa State University

Order Number 8909121

Development of a two-dimensional finite element soil-moisture flow model

Ahmed, Mushtaque, Ph.D.

Iowa State University, 1988

U·M·I
300 N. Zeeb Rd.
Ann Arbor, MI 48106

Development of a two-dimensional finite element soil-moisture flow model

by

Mushtaque Ahmed

A Dissertation Submitted to the
Graduate Faculty in Partial Fulfillment of the
Requirements for the Degree of
DOCTOR OF PHILOSOPHY

Department: Civil and Construction Engineering
Major: Water Resources

Approved:

Signature was redacted for privacy.

In Charge of Major Work

Signature was redacted for privacy.

For the Major Department

Signature was redacted for privacy.

For the Graduate College

Iowa State University
Ames, Iowa

1988

TABLE OF CONTENTS

LIST OF FIGURES

LIST OF TABLES

CHAPTER 1. INTRODUCTION

Water movement in the subsurface is one of the most complicated processes in the hydrologic cycle. Studies of the movement of water through porous material have been documented for the past 130 years (Wells, 1978). At present, the state-of-the-art allows investigation of problems involving saturated and unsaturated flow under a variety of conditions, and there is a greater recognition of the role of unsaturated flow in the moisture dynamics of soil profiles.

The understanding of water movement in soils is important in many practical problems. Water management agencies have need of improved estimates of groundwater recharge for defining sustainable withdrawals of water from aquifer systems for use in water permit allocation and review. Environmental quality agencies need knowledge of quantities and direction of flow in saturated-unsaturated flow systems for assessment of rates and timing of transport of nitrate-nitrogen and other agricultural chemicals and movement of contaminants from waste disposal sites or hazardous spills toward groundwater systems. There is also a need for tools for predicting the magnitude and transientness of the unsaturated flow field in order to establish guidelines for lysimeter placement and water sampling points beneath disposal and spill sites. Also, in order to determine irrigation requirements, wastewater land application rates, pumping rates, groundwater recharge rates, agricultural drainage requirements, and others, it is necessary to understand the flow mechanism in the soils both in the saturated and unsaturated zones (Chung, 1985).

Much research effort has been expended and many computer models have been formulated in efforts to simulate and understand various portions of the hydrologic cycle and hydraulic and soil erosion processes. Many current hydrologic models have been used to describe infiltration and runoff from individual storm events. However, most of these models make general assumptions concerning soil moisture movement and recharge to groundwater systems. Only a relatively few models have been developed which simulate water infiltration, unsaturated soil moisture movement, and crop moisture extraction in sufficient detail to even roughly predict groundwater recharge in areas where rainfall may limit surface evapotranspiration. These models include the SPAW (Soil Plant Air Water) model by Saxton et al. (1974), a finite difference model by Nimah and Hanks (1973), a finite element model by Neuman et al. (1974), a finite difference model by Feddes et al. (1978), and a water balance model developed by Anderson (1975; Anderson et al., 1978) and modified and applied by Shahghasemi (1980) and Shahvar (1981).

In the past few years, it has become clear to groundwater hydrologists that the simulation of groundwater flow regimes often is best accomplished within a stochastic framework rather than in the traditional deterministic framework. Underlying the move toward stochastic simulation is the realization that hydrogeological environments are exceedingly heterogeneous and, even in areas where considerable data are available, we can never uncover the exact spatial variation of the heterogeneous elements (Smith and Freeze, 1979a). Spatial variability of soil water properties has been

introduced in groundwater hydrology and soil physics since the 1960s and more intensively since the late 1970s.

In this study, a water balance model incorporating a two-dimensional finite element groundwater flow model of the saturated-unsaturated zone is presented. This model takes into consideration different hydrologic parameters such as rainfall, soil evaporation, crop transpiration, interception, infiltration, depression storage, and surface runoff. Given appropriate boundary conditions, the model will also predict tile outflow and deep percolation. To handle the stochastic properties of the hydraulic conductivity, the Monte Carlo simulation technique was used.

Objectives

The objective of this research was to develop a finite element model to simulate two-dimensional transient water flow through the saturated-unsaturated zone. The model was to have the capability to predict the pressure head and water content in the soil profile and to predict tile outflow and groundwater recharge considering the stochastic nature of the saturated hydraulic conductivity of soil.

The specific objectives were to (1) develop a water balance model incorporating a two-dimensional finite element saturated-unsaturated flow model with techniques to estimate rate and timing of soil evaporation, crop transpiration, soil infiltration, interception, depression storage, surface runoff, tile outflow, deep percolation, and saturated or unsaturated movement of moisture within the soil profile; and (2) verify the model with field data.

CHAPTER 2. LITERATURE REVIEW

Flow through soil is a very complex process affected by both soil and fluid properties. Flow systems can be divided into two categories: saturated flow and unsaturated flow. Saturated flow occurs when all the pores in the soil are filled with water, i.e., soil is completely saturated and there exists a potential gradient. Flow takes place in the direction of decreasing potential, and the rate of flow (flux) is proportional to the potential gradient and is affected by the geometric properties of the pore channel through which flow takes place. These principles hold true for unsaturated flow as well; but, in unsaturated flow, all the pores are not filled with water. Air is present in some of the pores.

The most important difference between unsaturated and saturated flow is in the hydraulic conductivity (Hillel, 1982). Hydraulic conductivity is the proportionality constant in the Darcy equation.

$$v = -K\frac{dH}{dL} \tag{2.1}$$

where

v = specific discharge,

dH/dL = hydraulic gradient,

H = hydraulic head, and

K = hydraulic conductivity.

When the soil is saturated, all the pores are filled with water so that there is fluid continuity. When soil becomes unsaturated, some of the pores become air filled and the conductive portions of the soil's cross

sectional area decreases correspondingly. Also, as drainage proceeds, the first pores to empty are the largest ones, which are the most conductive, leaving water to flow only in the smaller pores. Thus, the transition from saturation to unsaturation conditions generally entails a steep drop in hydraulic conductivity, which may decrease by several orders of magnitude (sometimes down to 1/100,000 of its value at saturation) as suction increases from 0 to 1 bar (Hillel, 1982).

The importance of unsaturated flow is quite obvious, as most processes involving soil-water interactions in the field, and particularly the flow of water in the rooting zone of most crop plants, occur while the soil is in an unsaturated condition. Although neglected (avoided) before, unsaturated flow in recent years has become one of the most important topics of research. The reason for past neglect is that unsaturated flow processes entail changes in the state and content of soil water during flow. Such changes involve complex relations among the variable soil moisture, moisture tension and conductivity, whose interrelations may be further complicated by hysteresis.

In general, there are three different approaches for analyzing water flow in porous media (Bear, 1972). They are molecular, microscopic, and macroscopic approaches. The molecular level transport theory is developed based on the movement of molecules, the microscopic level transport theory is developed by utilizing the continuum approach, and the macroscopic level

transport theory is developed by replacing microscopic variables by their volume average (Chung, 1985).

Experimental and theoretical evidences show that water can flow through porous media under the influence of gradients other than that of hydraulic head. The presence of a temperature gradient can result in groundwater flow (as well as heat flow) even when hydraulic gradients do not exist (Philip and de Vries, 1957). An electrical gradient can create a flow of water from high voltage to low when earth currents are set up in a soil. Chemical gradients can cause the flow of water (as well as the movement of chemical constituents through the water) from regions where water has higher salinity to regions where it has lower salinity, even if no other gradient is present.

Unsaturated flow is a special case of multiphase flow through porous media, with two phases, air and water, coexisting in the pore channels. The single-phase approach to unsaturated flow leads to techniques of analysis that are accurate enough for almost all practical purposes; but, there are some unsaturated flow problems where the multiphase flow of air and water must be considered. These commonly involve cases where a build-up in air pressure in the entrapped air ahead of a wetting front affects the movement of the front. More about multiphase flow in unsaturated flow is available in Wilson and Luthin (1963), Youngs and Peck (1964), McWhorter (1971), Bianchi and Haskell (1966), Green et al. (1970), and Freeze and Cherry (1979).

Theories on Saturated-Unsaturated Flow

The basic law of flow in both the saturated and unsaturated system is Darcy's Law and, when it is combined with the equation of continuity that describes the conservation of fluid mass during flow through a porous medium, a partial differential equation of flow can be defined. It has been said before that Darcy's Law holds for both saturated flow and unsaturated flow. In fact, Darcy's Law is also valid for steady-state flow and for transient flow, for flow in aquifers and for flow in aquitards, for flow in homogeneous systems and for flow in heterogeneous systems, for flow in isotropic media and for flow in anisotropic media, and for flow in both rocks and granular media (Freeze and Cherry, 1979). Thus, Darcy's Law provides an accurate description of the flow of groundwater in almost all hydrogeological environments. Darcy's Law is valid as long as the Reynolds number based on average grain diameter does not exceed some value between 1 and 10 (Bear, 1972).

The widely accepted theory regarding the flow of water in porous media proposes that the flow exhibits continuity across the boundary between saturated and unsaturated flow (water table). Experimental results have shown (Fujioka and Kitamura, 1964) that there is no sudden change of pressure at the boundary between the saturated zone and unsaturated zone of soil water. One theory differentiates between flow in the saturated zone and flow in the unsaturated zone. According to this theory, water in the unsaturated zone is assumed to have compressibility, while water in the saturated zone is assumed to be incompressible. Therefore, the propagation of pore pressure should suddenly change at the boundary between the

saturated and unsaturated soil profile and consequently the law of movement of soil water above and below the water table is distinctly different. Accepting this theory of discontinuity, the transient saturated-unsaturated interface constitutes an internal moving boundary (Chung, 1985).

In the present study, the theory of continuity of hydraulic head at the saturated-unsaturated interface is adopted.

The Groundwater Flow Equation

In almost every field of science and engineering, the techniques of analysis are based on an understanding of the physical processes, and in most cases, it is possible to describe these processes mathematically. Groundwater flow is no exception. In this section, a brief description about the development of the three dimensional transient groundwater flow equation for both saturated and unsaturated conditions will be presented.

Transient saturated flow

Consider a unit volume of porous media such as that shown in Figure 2.1. The law of conservation of mass for transient flow in a saturated porous medium requires that the net rate of fluid mass flow into any elemental control volume be equal to the time rate of change of fluid mass storage within the element. With reference to Figure 2.1, the equation of continuity (which describes the conservation of fluid mass during flow through a porous medium) takes the form:

$$\frac{\partial}{\partial x}(\rho v_x) + \frac{\partial}{\partial y}(\rho v_y) + \frac{\partial}{\partial z}(\rho v_z) = \frac{\partial(\rho n)}{\partial t} \qquad (2.2)$$

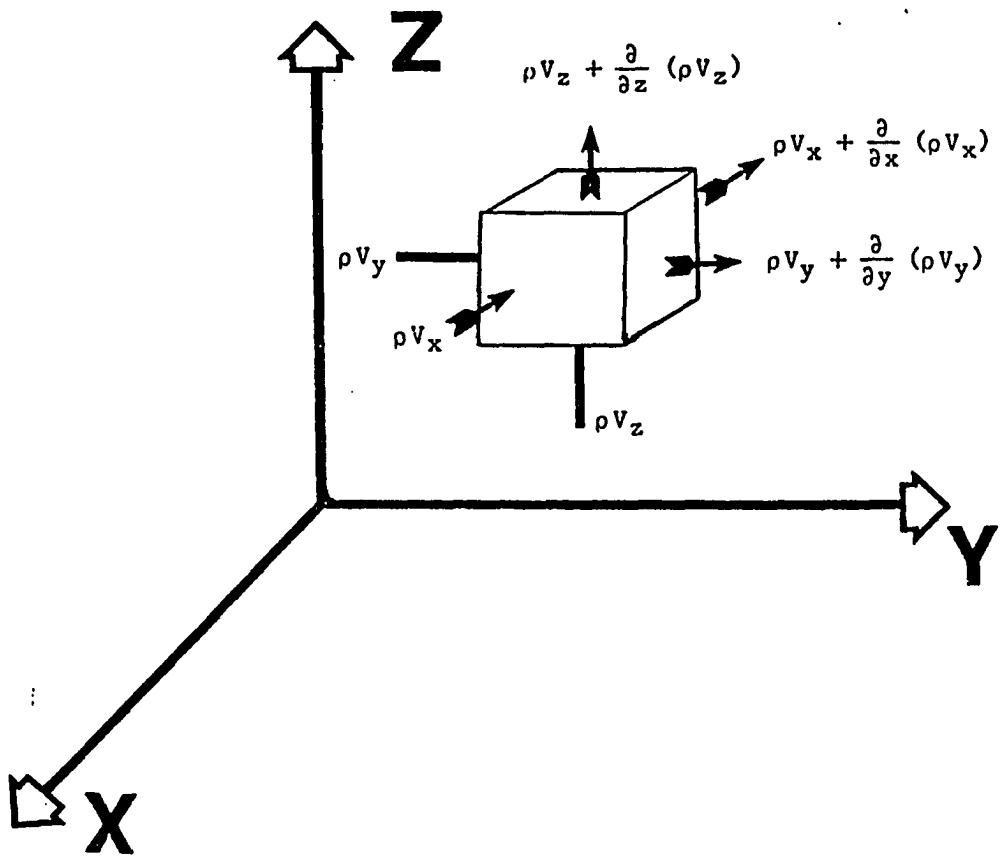

Figure 2.1. Elemental control volume for flow through porous media

where

ρ = density of the fluid,

n = porosity, and

v = specific discharge.

Expanding the right hand side

$$\frac{\partial}{\partial x}(\rho v_x) + \frac{\partial}{\partial y}(\rho v_y) + \frac{\partial}{\partial z}(\rho v_z) = n\frac{\partial \rho}{\partial t} + \rho\frac{\partial n}{\partial t} \tag{2.3}$$

The first term on the right-hand side of equation (2.3) is the mass rate of water produced by an expansion of the water due to a change in its density, ρ. The second term is the mass rate of water produced by the compaction of the porous medium as reflected by the change in its porosity, n. The change in ρ and the change in n are both produced by a change in hydraulic head, H, and the volume of water stored by the two mechanisms for a unit decline in head is S_s, specific storage. Thus, the mass rate of water stored (time rate of change of fluid mass storage) is $\rho S_s\ \partial H/\partial t$, and equation (2.3) becomes

$$\frac{\partial}{\partial x}(\rho v_x) + \frac{\partial}{\partial y}(\rho v_y) + \frac{\partial}{\partial z}(\rho v_z) = \rho S_s \frac{\partial H}{\partial t} \tag{2.4}$$

The terms of the form $\rho \partial v_x/\partial x$ are much greater than terms of the form $v_x\ \partial\rho/\partial x$. Thus ρ can be eliminated from both sides of equation (2.4). Inserting Darcy's law gives:

$$\frac{\partial}{\partial x}\left(K^s_x \frac{\partial H}{\partial x}\right) + \frac{\partial}{\partial y}\left(K^s_y \frac{\partial H}{\partial y}\right) + \frac{\partial}{\partial z}\left(K^s_z \frac{\partial H}{\partial z}\right) = S_s \frac{\partial H}{\partial t} \tag{2.5}$$

where K^s_x, K^s_y and K^s_z are the saturated hydraulic conductivity in x, y and z directions, respectively. This is the equation of flow for transient flow through a saturated anisotropic nonhomogeneous porous medium.

Transient unsaturated flow

We can define the degree of saturation, θ', as $\theta' = \theta/n$, where n is the porosity. For flow in an elemental control volume that may be only partially saturated, the equation of continuity must reveal the time rate of change of moisture content as well as the time rate of change of storage due to water expansion and aquifer compaction. The ρn term in equation (2.2) must become $\rho n\theta'$, and equation (2.2) becomes

$$\frac{\partial}{\partial x}(\rho v_x) + \frac{\partial}{\partial y}(\rho v_y) + \frac{\partial}{\partial z}(\rho v_z) = n\theta' \frac{\partial \rho}{\partial t} + \rho\theta' \frac{\partial n}{\partial t} + n\rho \frac{\partial \theta'}{\partial t} \qquad (2.6)$$

For unsaturated flow, the first two terms on the right-hand side of equation (2.6) are generally much smaller than the third term. Neglecting the first two terms, cancelling the ρ's from both sides, inserting the unsaturated form of Darcy's Law, and recognizing that $nd\theta' = d\theta$, leads to

$$\frac{\partial}{\partial x}\left[K_x(h) \frac{\partial H}{\partial x}\right] + \frac{\partial}{\partial y}\left[K_y(h) \frac{\partial H}{\partial y}\right] + \frac{\partial}{\partial z}\left[K_y(h) \frac{\partial H}{\partial z}\right] = \frac{\partial \theta}{\partial t} \qquad (2.7)$$

Noting that specific moisture capacity $C = d\theta/dh$ and $H = h + z$, (h = pressure head, z = gravitational head) we get

$$\frac{\partial}{\partial x}\left[K_x(h) \frac{\partial h}{\partial x}\right] + \frac{\partial}{\partial y}\left[K_y(h) \frac{\partial h}{\partial y}\right] + \frac{\partial}{\partial z}\left[K_z(h)\left(\frac{\partial h}{\partial z} + 1\right)\right] = C(h) \frac{\partial h}{\partial t} \qquad (2.8)$$

Equation (2.8) is the h based equation of flow for transient flow through an unsaturated porous medium. If we replace $K(h) = K^r(h)\, K^s$ where

$K^r(h)$ = relative hydraulic conductivity,

$$= \frac{K(h)}{K^s}$$

equation (2.8) becomes

$$\frac{\partial}{\partial x}\left[K^r(h)K^s{}_x \frac{\partial h}{\partial x}\right] + \frac{\partial}{\partial y}\left[K^r(h)K^s{}_y \frac{\partial h}{\partial y}\right] + \frac{\partial}{\partial z}\left[K^r(h)K^s{}_z \frac{\partial h}{\partial z}\right] + \frac{\partial}{\partial z}\left[K^r(h)K^s{}_z\right]$$

$$= C(h) \frac{\partial h}{\partial t} \qquad (2.9)$$

For saturated condition, equation (2.9) can be expressed as

$$\frac{\partial}{\partial x}\left(K^s{}_x \frac{\partial h}{\partial x}\right) + \frac{\partial}{\partial y}\left(K^s{}_y \frac{\partial h}{\partial y}\right) + \frac{\partial}{\partial z}\left(K^s{}_z \frac{\partial h}{\partial z}\right) + \frac{\partial}{\partial z}\left(K^s{}_z\right) = S_s \frac{\partial h}{\partial t} \qquad (2.10)$$

Neuman and Davis (1983) expressed both saturated and unsaturated flow in a single equation

$$\frac{\partial}{\partial x}\left[K^r(h)K^s{}_x \frac{\partial h}{\partial x}\right] + \frac{\partial}{\partial y}\left[K^r(h)K^s{}_y \frac{\partial h}{\partial y}\right] + \frac{\partial}{\partial z}\left[K^r(h)K^s{}_z \frac{\partial h}{\partial z}\right]$$

$$+ \frac{\partial}{\partial z}\left[K^r(h)K^s{}_z\right] - \left[C(h) + \beta S_s\right]\frac{\partial h}{\partial t} - S = 0 \qquad (2.11)$$

where S is a sink/source term. For saturated condition, $K^r(h) = 1$, $C(h) = 0$, and $\beta = 1$. For unsaturated condition, $\beta = 0$. For two-dimensional (x,z) cases, the second term of the left-hand side of the equation (2.11) should be neglected.

In this section, the governing equation has been derived using the h-based instead of θ-based. Milly and Eagleson (1980) discussed the differences between the two approaches. The advantages of the h-based equation are:

1. it is applicable in both the unsaturated and saturated zones, and
2. the flux expression is simpler (Chung, 1985).

Hydrologic Processes

To solve the soil water flow equation (2.11), the boundary conditions must be fixed. For a vertical two-dimensional flow system, the top boundary is an atmospheric boundary which is along the soil-air interface

on the top of the soil. Either evaporation or infiltration occurs in this boundary. The amount of infiltration is dependent on many factors; such as, amount, duration, and intensity of rainfall, interception, surface runoff, etc. For evaporation, the actual evaporation rate across the top boundary is governed by soil water conditions, such as moisture content at the top layer, while the potential rate is controlled by atmospheric conditions. In this chapter, a brief description about interception, surface runoff, infiltration, evapotranspiration, deep percolation, and tile outflow will be provided.

Interception

Interception is defined as the process whereby precipitation is retained on the leaves, branches, and stems of vegetation and on the litter covering the ground. From there, it is evaporated without adding to moisture storage of the soil. The vegetation canopy is the surface of vegetation that can intercept precipitation. Crop Leaf Area Index (CLAI) is a measure of canopy density. CLAI will vary from one vegetation type to another, for example, from grassland to corn. The interception process can be represented as a storage of finite capacity. When evaporation is greater than the rainfall, a loss of moisture will take place from the interception storage. This loss will continue until the interception storage is exhausted. Where precipitation is in excess of evaporation, the interception storage will fill until its capacity is exceeded. Water in excess of interception storage will reach the ground surface. This will result in infiltration and may also cause surface runoff.

Surface runoff

Surface runoff occurs only when the rainfall rate is greater than the infiltration rate. In fact, surface runoff occurs after the initial demands of interception, infiltration, and surface storage have been satisfied. Surface runoff varies during a rainfall event and ends during or soon after rainfall stops. Surface runoff is a function of both surface and soil conditions.

Infiltration

Infiltration is the term applied to the process of water entry into the soil, generally by downward flow through all or part of the soil surface. The rate of this process, relative to the rate of water supply, determines how much water will enter the root zone, and how much, if any, will run off (Hillel, 1982). Infiltration is influenced by soil properties (e.g., hydraulic conductivity), rainfall (or irrigation) intensity, initial water content, soil surface condition, presence of impeding layer inside the profile, etc. Much research has been done and many equations have been developed on this subject. Green and Ampt (1911) developed the first physically based infiltration equation.

The many equations developed on infiltration can be classified as either theoretical or empirical. Table 2.1 (after Chung, 1985) shows various infiltration equations. Many of the original equations have been modified to make them usable under different conditions. Holtan et al. (1967) developed an iterative computational procedure for the modified Holtan's equation to determine the incremental infiltration for a time

Table 2.1. Infiltration equations

Name	Equation	
Green and Ampt	$i = i_c + A/I$	theoretical
Philip	$i = i_c + \frac{s}{2}t^{-\frac{1}{2}}$	theoretical
Kostiakov	$i = Bt^{-m}$	empirical
Horton	$i = i_c + (i_0 - i_c)\, e^{-kt}$	empirical
Holtan	$i = i_c + a(M - I)^n$	empirical
Modified Holtan	$i = i_c + a(\frac{S - I}{T})^p$	empirical
Modified G-A	$i = A + B/I$	theoretical
Modified G-A	$i = K\,(1 + \frac{M_d\, S_h}{I})$	theoretical

A, B, a, k, m, n, p = parameters depending on soil properties

i = infiltration rate

i_c = steady state infiltration rate

i_0 = initial infiltration rate

I = accumulated infiltration

t = time from the beginning of infiltration

s = sorptivity

M = water storage capacity of soil

S = water storage potential above any impeding strata

T = total pore volume above any impeding strata

M_d = initial soil moisture deficit

S_h = average suction head at the wetting front

K = hydraulic conductivity

period. This procedure has been used by DeBoer (1969), Anderson (1975), Shahghasemi (1980), and Chung (1985).

Neuman and Davis (1983), in their finite element model, used an iterative procedure where infiltration takes place only due to pressure gradient. This process will be further discussed in Chapter 3.

Evapotranspiration

Many models are available for predicting potential evapotranspiration (PET). Potential evapotranspiration (PET) is the evapotranspiration which occurs when a healthy growing crop cover completely covers the ground surface, is of uniform height, and at no time is short of water or subjected to moisture stress.

Potential evapotranspiration depends on climatological factors such as solar radiation, air temperature, humidity, and wind velocity. Lysimeters are used for measurement of actual evapotranspiration. Shaw (1963) concluded that of the various methods available, pan evaporation was probably the most generally available in Iowa, but the Penman equation gave the most reliable daily values when the data were available. A summary of the models for predicting PET including required input data is given in Skaggs (1978).

Penman equation

A modified Penman equation was used by Anderson (1975). The Penman equation is:

$$PET = \frac{\delta/\gamma}{\delta/\gamma + 1}(R_n - G) + \frac{1}{\delta/\gamma + 1}(15.36)(1 - 0.01\ W)(e_s - e_d) \qquad (2.12)$$

where

PET = potential evapotranspiration (Langleys/day),

δ = slope of the saturation vapor pressure - temperature curve (mb/°C),

γ = psychrometric constant (mb/°C),

R_n = net radiation (Langleys/day)

G = soil heat flux (Langleys/day),

W = daily total wind travel (miles),

e_s = saturation vapor pressure at the mean daily air temperature (mb), and

e_d = saturation vapor pressure at the mean dew-point temperature (mb).

Equation 2.12 requires daily values of air temperature, relative humidity, wind movement, and net solar radiation. Net solar radiation can be calculated using the following equations (Anderson, 1975):

$$R_{so} = 547 + 227 \sin (2\pi X/365 - \pi/2) \tag{2.13}$$

$$R_{bo} = 0.98 - (0.66 + 0.044 \sqrt{e_d}) (5.855 \times 10^{-8}) (T^4_{2A} - T^4_{1A}) \tag{2.14}$$

$$R_b = (1.35 R_s/R_{so} - 0.35) R_{bo} \tag{2.15}$$

$$R_n = (1 - \alpha) R_s - R_b \tag{2.16}$$

$$\alpha = a - b \times CLAI, \quad CLAI \leq 4.0 \tag{2.17}$$

where

R_{so} = maximum clear day solar radiation (Langleys),

X = adjusted day of the year such that the maximum radiation occurs 18 days before mid-year,

R_{bo} = net outgoing longwave radiation on a clear day (Langleys/day),

T_{2A} = maximum daily temperature (degrees K),

T_{1A} = minimum daily temperature (degrees K),

R_b = net outgoing longwave radiation (Langleys/day),

R_s = measured solar radiation on a given day (Langleys),

α = surface albedo,

a = bare soil albedo,

b = 0.25 (crop albedo - a), and

CLAI = crop leaf area index, leaf area per unit field area defined to include dead and dormant leaves which are still attached to the plant.

Details of these equations are available in Anderson (1975), Jensen et al. (1971), and Ritchie (1972).

Soil heat flux was calculated using an equation given by Jensen et al. (1971):

$$G = (T_f - TPAST) \times 5.0 \qquad (2.18)$$

where

T_f = mean daily air temperature (degrees F), and

TPAST = average air temperature for the previous three days in °F.

To evaluate the ration δ/γ in Penman's equation, a polynomial equation is given by Saxton (1972).

$$\delta/\gamma = 0.672 + 0.0428\ T_c + 1.13 \times 10^{-3}\ T_c^2 + 1.66 \times 10^{-5}\ T_c^3 + 1.7 \times 10^{-7}\ T_c^4 \quad (2.19)$$

where

T_c = mean daily air temperature (degrees C).

To obtain potential daily evapotranspiration in cm of water, the value obtained from equation (2.12) is multiplied by 0.000673 x 2.54.

Considering the fact that all the data needed for the Penman equation are available at only very few locations, the simple PET models based on pan evaporation data have gained wide acceptance. Saxton et al. (1974) developed a linear regression equation to predict PET from the pan evaporation data. Shaw (1963), from his many years of field observation, has developed some equations to predict evapotranspiration in Iowa. Kanwar (1981) used Shaw's method. Shaw (1963) gives the following equations:

April 1 to April 19 period:

$$ET = 0.035 \text{ cm/day} \quad (2.20)$$

April 20 to June 26 period:

$$ET = PAN * RATIO \quad (2.21)$$

June 27 to July 31 period:

$$ET = PAN * RATIO * STRESS\ FACTOR \quad (2.22)$$

August 1 to day of harvest period:

$$ET = PAN * RATIO * STRESS\ FACTOR \quad (2.23)$$

where

ET = evapotranspiration,

PAN = open-pan evaporation,

RATIO = ratio of ET/PAN as a function of time (Fig. 2.2),

STRESS FACTOR = a factor based on percent available moisture and PAN (Figs. 2.3 and 2.4)

Figures 2.2, 2.3 and 2.4 provide information of RATIO and STRESS FACTORS.

Shahghasemi (1980) used the regression line developed by Saxton et al. (1974) to convert pan data (PAN) to PET

$$PET = 0.01 + 0.83\ (PAN) \tag{2.24}$$

where both PET and PAN are in inches.

Shahavar (1981) used the following relationships based on comparison between pan data and the Penman equation:

$$\text{June:}\quad PET = 0.149 + 0.405\ (PAN) \tag{2.25}$$

$$\text{July:}\quad PET = 0.140 + 0.497\ (PAN) \tag{2.26}$$

$$\text{August:}\quad PET = 0.153 + 0.396\ (PAN) \tag{2.27}$$

where both PET and PAN are in cm.

Tile outflow

Tile drainage is the artificial removal of excess water from within the soil by means of tubes placed at appropriate depths. This is done because excess water in the soil tends to block soil pores and thus retard aeration and, in effect, strangulate the roots. Water flows into tiles as

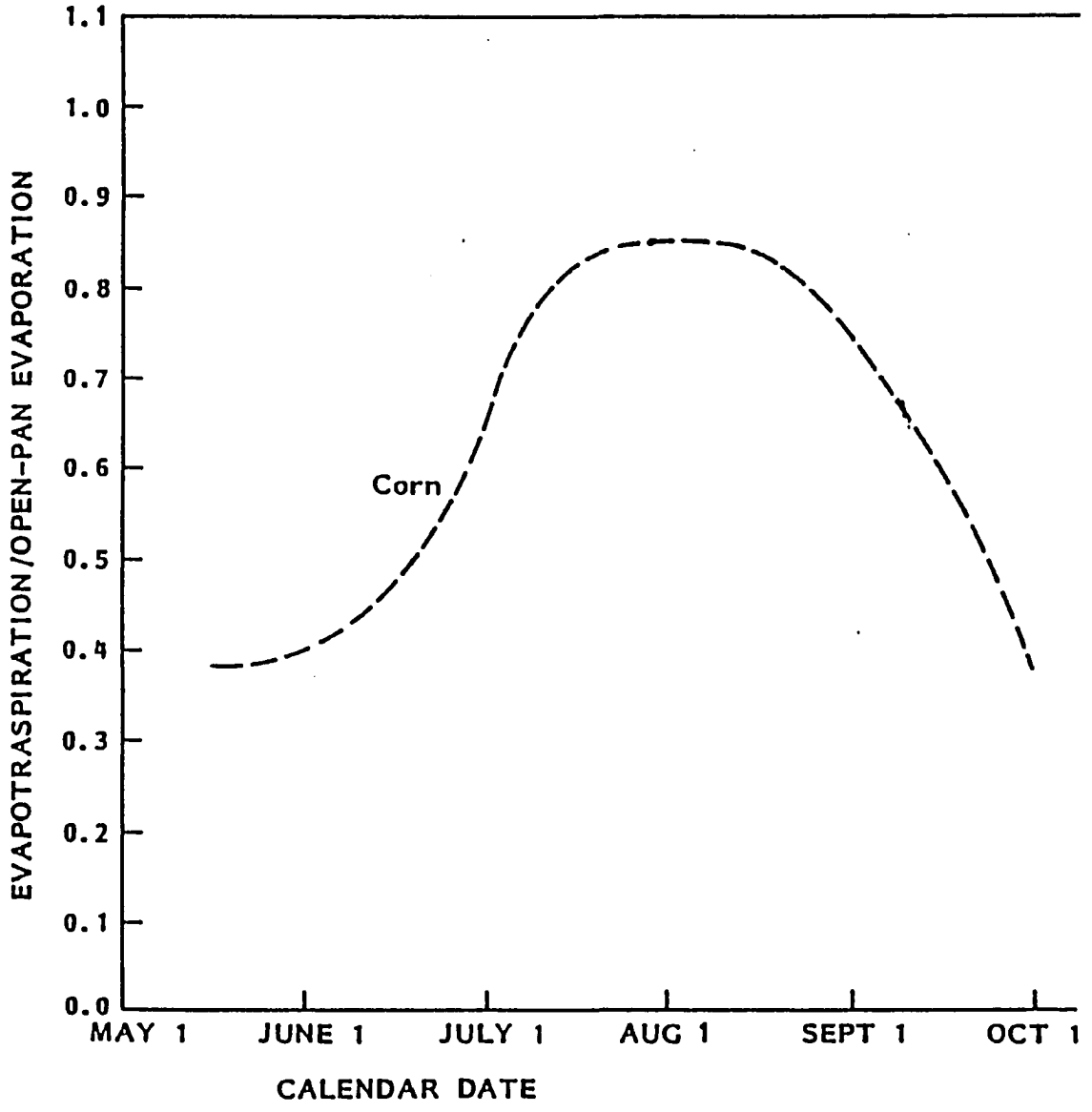

Figure 2.2. Ratio of evapotranspiration for corn compared to open-pan evaporation (Kanwar, 1981)

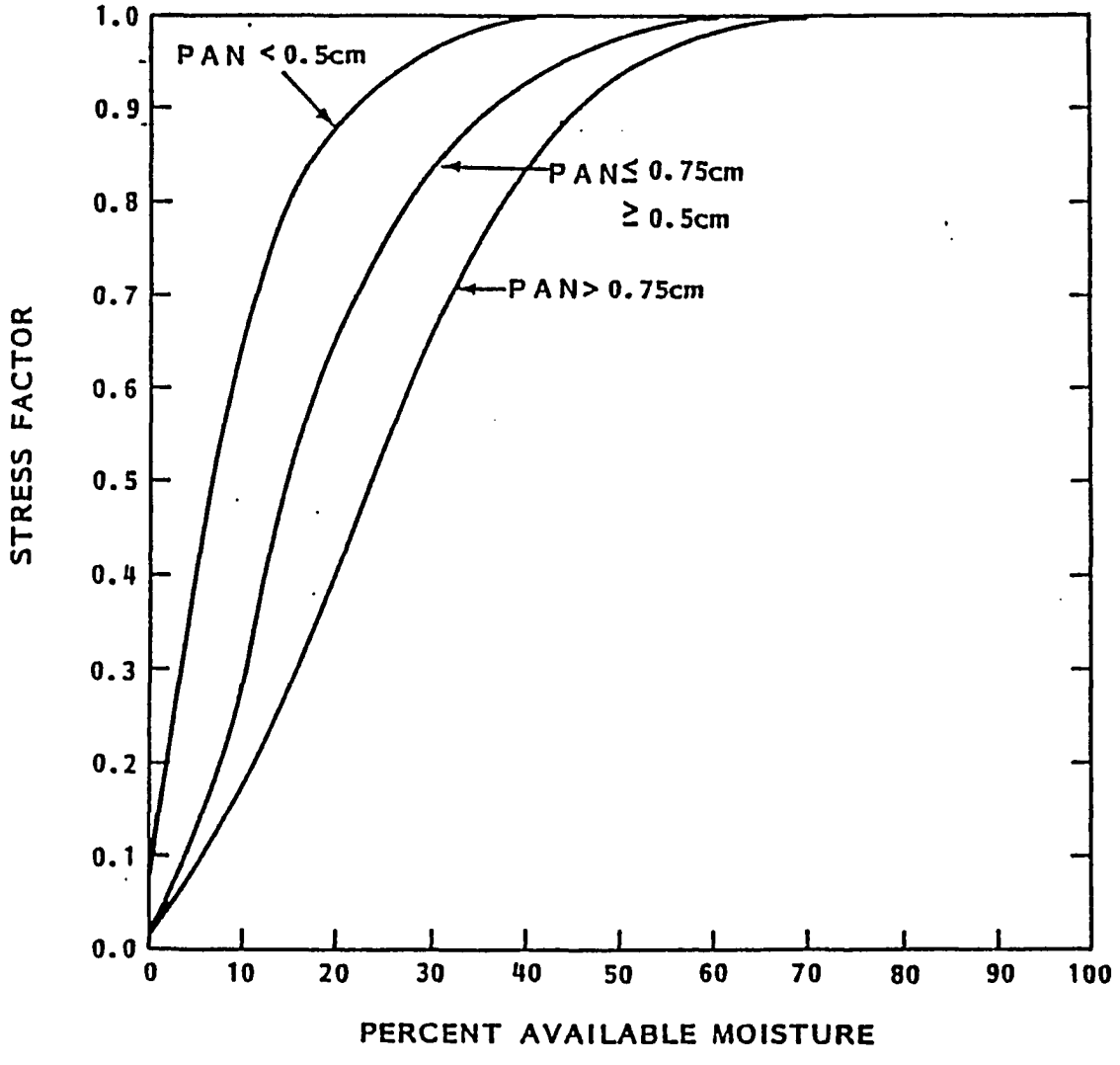

Figure 2.3. Relationship between stress factor and percent available moisture before August 1st (Kanwar, 1981)

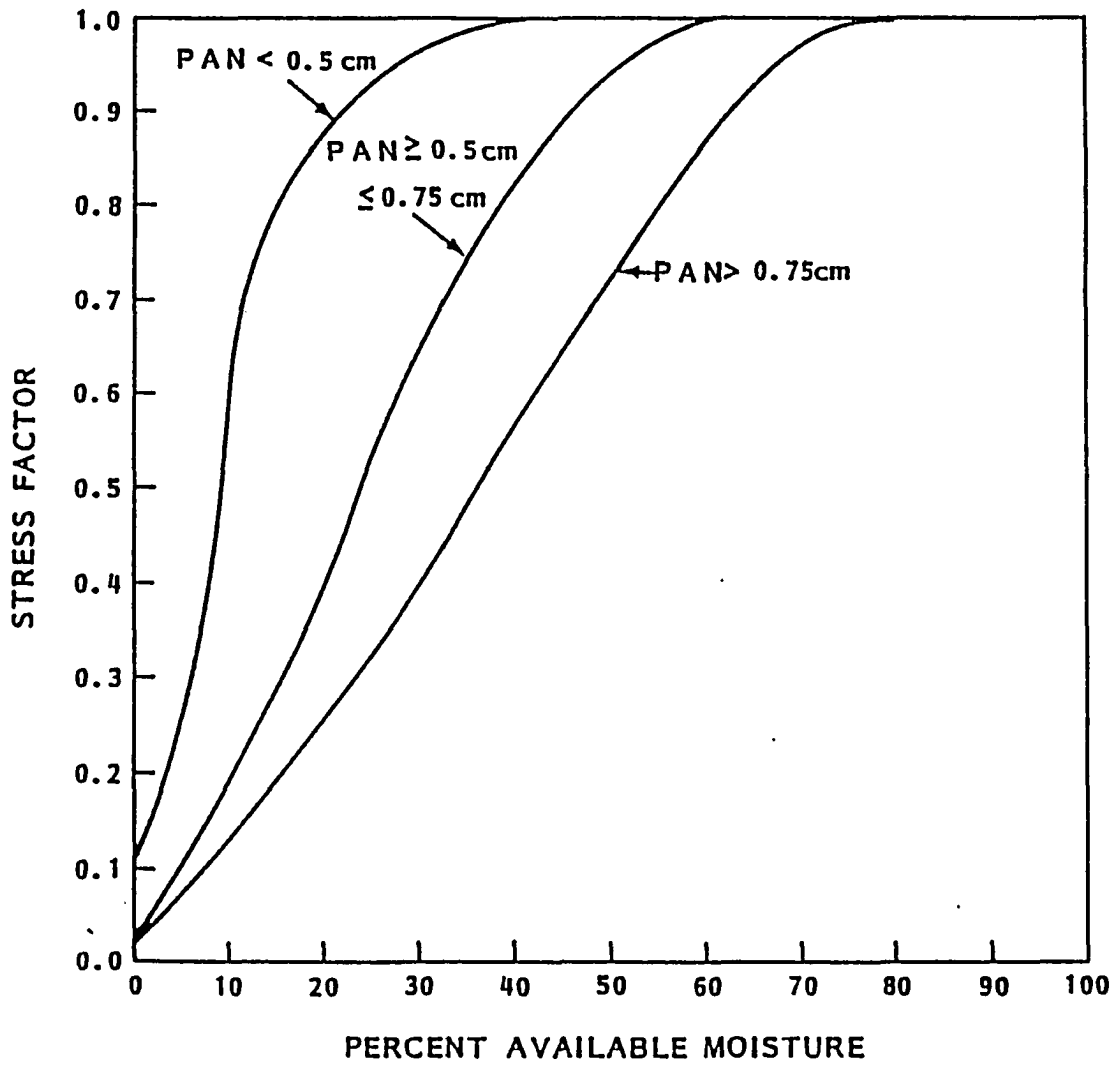

Figure 2.4. Relationship between stress factor and percent available moisture after July 31st (Kanwar, 1981)

a result of the hydraulic gradients existing in the soil. Flow rate into the tiles depends on the following factors:

1. hydraulic conductivity of the soil,
2. configuration of the water table and hydraulic pressure of the groundwater,
3. depths of the tiles, relative to the groundwater table,
4. slopes of the tiles and their outlet elevation,
5. horizontal spacing between tiles,
6. character of the drains, whether open ditches or tubes,
7. inlet openings in the tiles,
8. envelope materials,
9. diameter of the drains, and
10. the rate at which water is added to groundwater.

It should be mentioned here that water does not spontaneously flow out of the soil into a tile unless the pressure of soil water is greater than atmospheric. For this reason, tiles must be located below the water table to draw water and the water table cannot be lowered below the drains. Thus, the depth and spacing of drains is of crucial importance (Hillel, 1982).

Many equations, empirically or theoretically based, have been developed for the purpose of determining the desirable depths and spacing of tiles in different soil and groundwater conditions. These are mostly based on very simplifying assumptions. One such well-known equation is that of Hooghoudt. Hillel (1982) describes this equation in detail. Neuman and Davis (1983), in their two-dimensional finite element flow

seepage face (nodes) to create the condition for tile outflow, when these nodes are saturated (i.e., tile is flowing), the nodes are prescribed to have zero pressure head and the finite element solution is obtained and outflow is calculated. When unsaturated (no tile outflow), these tile nodes are prescribed as no flow nodes and pressure head is calculated based on the finite element solution.

Deep percolation

Deep percolation, which is used to represent the flux across the bottom boundary whether it is saturated or not, is not easy to measure directly. It can be measured employing a weighing lysimeter. A water budget method can also be used to determine bottom flux. It also can be calculated from the hydraulic gradient obtained from piezometers at different depths (Chung, 1985). Fleming (1975) defines deep percolation as the process whereby water enters deep inactive groundwater storage, which does not discharge at the catchment outlet.

Soil Properties

Moisture movement in soil is influenced by soil parameters like porosity, water content, pressure head, hydraulic conductivity, texture, etc.

Porosity

$$n = V_f/V_t = \frac{V_a + V_w}{V_s + V_a + V_w} \qquad (2.28)$$

where

n = porosity,

V_f = volume of pores,

V_t = total volume of sample,

V_a = volume of air,

V_w = volume of water, and

V_s = volume of solids.

The porosity is an index of relative pore volume in the soil. Its value generally lies in the range 0.3 - 0.6 (30 - 60%). Coarse-textured soils tend to be less porous than fine-textured soils, though the mean size of individual pores is greater in the former than in the latter (Hillel, 1982). Porosity can also be expressed in terms of soil bulk density:

$$n = 1 - \rho_b/\rho_s \tag{2.29}$$

where

ρ_b = dry bulk density, and

ρ_s = density of the solids.

Water content

The wetness, or relative water content, of soil can be expressed in various ways: relative to the mass of solids, relative to the total mass, relative to the volume of solids, relative to the total volume, and relative to the volume of pores. Volume wetness (θ) is also termed as volumetric water content or volume fraction of soil water. It is computed as a percentage of the total volume of the soil:

$$\theta = V_w/V_t = \frac{V_w}{V_s + V_f} \qquad (2.30)$$

In sandy soils, the value of θ at saturation is on the order of 40-50%; in medium-textured soils, it is approximately 50%; and in clayey soils, it can approach 60% (Hillel, 1982).

Measurement of soil water content

There are direct and indirect methods to measure soil water content. The traditional (gravimetric) methods of measuring mass wetness consists of removing a sample by augering into the soil and then determining its moist and dry weights. This method is laborious and time consuming. The sampling method is destructive and may disturb an experimental plot sufficiently to distort the results (Hillel, 1982). The electrical resistance block method is based upon the theory that the electrical resistance of a porous block placed in the soil depends upon the soil water content. This method can be used to obtain a continuous indication of soil moisture changes in situ. Neutron scattering method is an efficient and reliable technique for monitoring soil moisture in the field. This method is less laborious, more rapid than others and nondestructive. The main disadvantages are the high initial cost of the instrument, low degree of spatial resolution, difficulty of measuring moisture in the soil surface zone, and the health hazard associated with exposure to neutron and gamma radiation (Hillel, 1982). The neutron moisture meter consists of two main parts: a probe, which is lowered into an access tube inserted vertically into the soil, and a scaler or ratemeter to monitor the flux of slow neutrons scattered by the soil. Additional approaches to the measurement

of soil wetness include gamma ray absorption, the dependence of soil thermal properties upon water content, and the use of ultrasonic waves, radar waves, and dielectric properties.

Soil water potential

In the study of moisture movement in soil, the term soil water potential is a very important one. Water flows from higher potential energy to lower potential energy level. It is not the absolute amount of potential energy contained in the water which is important in itself, but rather the relative level of that energy in different regions within the soil. A soil physics terminology committee of the International Soil Science Society (Aslyng, 1963) defined the total potential of soil water as "the amount of work that must be done per unit quantity of pure water in order to transport reversibly and isothermally an infinitesimal quantity of water from a pool of pure water at a specific elevation at atmospheric pressure to the soil water (at the point under consideration)." Soil water is subject to a number of force fields, causing its potential to differ from that of pure, free water. Thus, the total potential of soil water is considered as the sum of the separate contributions of various factors:

$$\phi_t = \phi_g + \phi_p + \phi_o + \ldots \tag{2.31}$$

where

ϕ_t = total potential,

ϕ_g = gravitational potential,

ϕ_p = pressure (or matric) potential, and

ϕ_o = osmotic potential.

Soil water potential can be expressed in terms of energy per unit mass, energy per unit volume, or energy per unit weight (hydraulic head). the latter is most commonly used.

Pressure potential

When soil water is at hydrostatic pressure greater than atmospheric, its pressure potential is considered positive. When it is at a pressure lower than atmospheric (also known as tension or suction), the pressure potential is considered negative. The pressure potential of soil water in unsaturated flow is caused by capillary attraction and adsorption. These forces attract and bind water in the soil and lower its potential energy below that of bulk water. Capillarity is due to the surface tension of water and its contact angle with the solid particles. Soil also exhibits adsorption, which forms hydration envelopes over the particle. These two mechanisms of soil water interaction are illustrated in Figure 2.5.

In general, the negative pressure potential results from the combined effect of the two mechanisms, which cannot easily be separated, since the capillary "wedges" are at a state of internal equilibrium with the adsorption "films," and the ones cannot be changed without affecting the others (Hillel, 1982).

Soil-moisture characteristic curve

Increasing soil moisture tension (suction) results in decreasing soil wetness. The amount of water remaining in the soil at equilibrium is a function of the sizes and volumes of the water-filled pores and hence it is a function of the matric suction. Soil-moisture characteristic curve is a

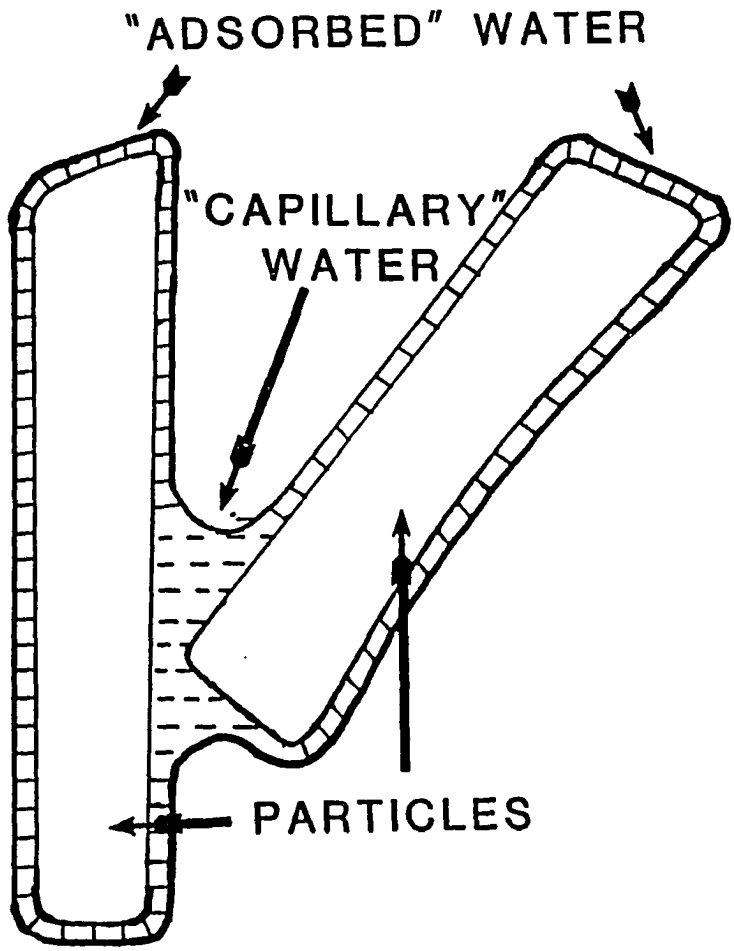

Figure 2.5. Water in an unsaturated zone under capillarity and adsorption (Hillel, 1982)

graphical representation of the relationship between soil water content and suction. Figure 2.6 shows such a relationship.

The amount of water retained at low values of matric suction (say, between 0 and 1 bar of suction) depends primarily upon the capillary effect and the pore-size distribution, and, hence, is strongly affected by the structure of the soil. Whereas, water retention in the higher suction range is due mostly to adsorption and is thus influenced less by the structure and more by the texture and specific surface of the soil material. In soil, the greater the clay content, the greater the water retention at any particular suction, and the more gradual the slope of the curve. In a sandy soil, most of the pores are relatively large, and once these large pores are emptied at a given suction, only a small amount of water remains.

Hysteresis

The relationship between pressure head and water content can be obtained in two ways: (1) by gradually drying an initially saturated soil, and (2) by gradually wetting an initially dry soil. Each of these two methods yields a continuous curve but these two curves will not be identical. The equilibrium water content at a given pressure (suction) is greater in drying than in wetting, as illustrated in Figure 2.7. This dependence of the equilibrium content and state of soil water upon the direction of the process leading up to it is called hysteresis.

The hysteresis effect may be attributed to several causes (Hillel, 1982):

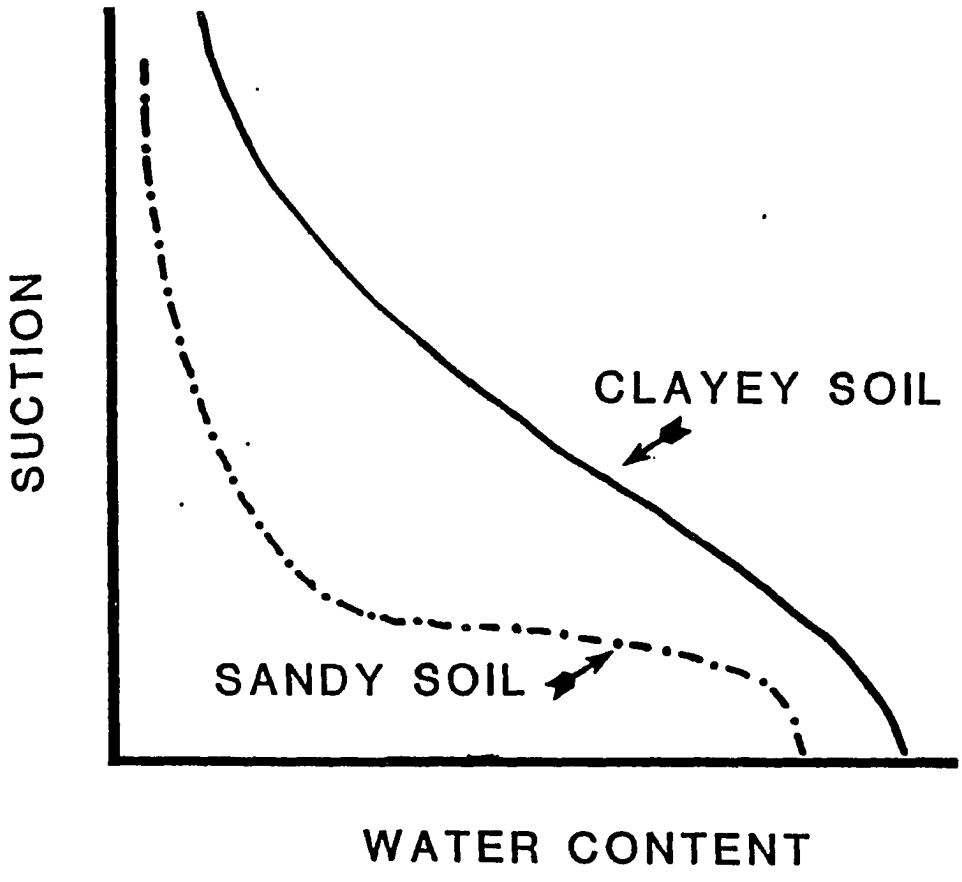

Figure 2.6. Soil-moisture characteristic curve

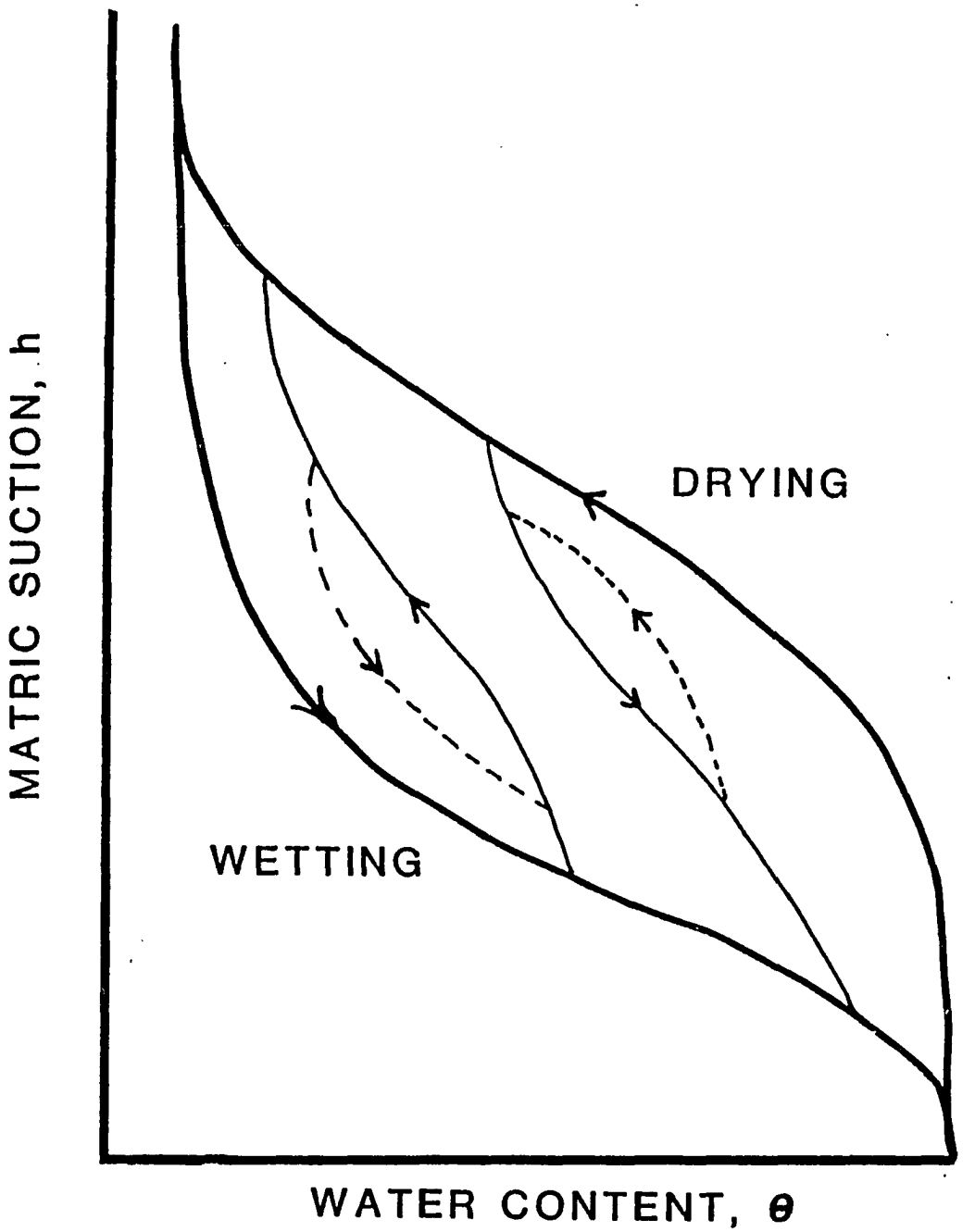

Figure 2.7. The hysteristic soil-moisture characteristic curve (Chung, 1985)

1. The geometric nonuniformity of the individual pores, resulting in the "ink bottle" effect;
2. The contact-angle effect, resulting from the fact that the contact angle of water on the solid walls of pores tends to be greater and hence the radius of curvature is greater in an advancing meniscus than in the case of a receding one. A given water content will tend, therefore, to exhibit greater suction in desorption than in sorption;
3. Entrapped air, which further decreases the water content of newly wetted soil; and
4. Swelling, shrinking, or aging phenomena, which result in differential changes of soil structure, depending on the wetting and drying history of the sample.

Because of its complexity, the hysteresis phenomenon is too often ignored, and the soil moisture characteristic which is generally reported is the desorption curve.

Hydraulic conductivity

In groundwater flow problems, knowledge of hydraulic conductivity is absolutely necessary. Hydraulic conductivity is a property of the conducting medium which measures its ability to transmit the liquid. Using Darcy's equation, we can say that hydraulic conductivity is the ratio of the flux to the hydraulic gradient. There are two terms for hydraulic conductivity: saturated and unsaturated hydraulic conductivity. Saturated hydraulic conductivity of the soil is the hydraulic conductivity of a fully saturated soil. Whereas, the unsaturated hydraulic conductivity of the

soil is the hydraulic conductivity at the unsaturated condition and is a function of the water contents.

In a saturated soil of stable structure, as well as in a rigid porous medium such as sandstone, the hydraulic conductivity is characteristically constant. But in many soils, the hydraulic conductivity does not, in fact, remain constant. Because of various chemical, physical, and biological processes, the hydraulic conductivity may change as water permeates and flows in a soil. Entrapped air may also affect conductivity. The hydraulic conductivity is not only dependent on soil but also on the fluid. The soil characteristics which affect hydraulic conductivity are the total porosity, the distribution of pore sizes, and tortuosity. The fluid density and viscosity affect conductivity. From a theoretical point of view, the hydraulic conductivity, K, can be separated into two factors: intrinsic permeability of the soil, k, and fluidity of the liquid or gas, f.

$$K = kf \tag{2.32}$$

where K is expressed in terms of cm/sec (LT^{-1}), k is expressed in cm^2 (L^2) and f in 1/(cm sec) ($L^{-1}T^{-1}$). Fluidity is inversely proportional to viscosity:

$$f = \rho g/\eta \tag{2.33}$$

where

η = viscosity (dyn sec/cm^2),

ρ = fluid density (gm/cm^3), and

g = gravitational acceleration (cm/sec^2).

Unsaturated hydraulic conductivity

From equation (2.11), it is obvious that information on the relationship of unsaturated hydraulic conductivity with either water content or pressure head is essential for solving unsaturated flow problems. But measuring the unsaturated hydraulic conductivity is time consuming and expensive (Van Genuchten, 1980). For this reason, indirect methods are widely used for determining unsaturated hydraulic conductivity.

Values of hydraulic conductivity are sensitive to small changes in water content (Nielsen et al., 1973). Hydraulic conductivity may in fact decrease by several orders of magnitude when soil becomes unsaturated from an initial saturated condition.

It should also be mentioned that unsaturated hydraulic conductivity shows hysteretic effects, especially as functions of pressure head.

Because of the difficulty in measuring hydraulic conductivity of a soil as a function of its water content, empirical and theoretical relationships between unsaturated hydraulic conductivity and either water content or pressure head have been proposed. Several empirical relationships have been developed from soil water characteristics curves (e.g., Brooks and Corey, 1964; Campbell, 1974). Table 2.2 (after Chung, 1985) contains some of these equations.

Table 2.2. Empirical equations relating hydraulic conductivity to water content or pressure head

Equation	Independent variable	Fitting parameters
$K(h) = a/h^n$	h	a, n
$K(h) = a/(b + h^n)$	h	a, b, n
$K(\Theta) = a\Theta^m$	Θ	a, m
$K(h) = K^s(h_a/h)^n$	h	n
$K(h) = K^s/\ 1 + (h/h_w)^m$	h	m
$K(h) = K^s \exp a(h - h_a)$	h	a
$K(\Theta) = K^s \left(\frac{\Theta - \Theta_r}{\Theta_s - \Theta_r}\right)^\gamma$	Θ	γ, Θ_r

h = soil water pressure (suction) head

Θ = volumetric water content

h_a = air entry value

h_w = water entry value

K^s = saturated hydraulic conductivity

Θ_s = saturated water content

Θ_r = residual water content

a, b, m, n, and γ = parameters to be determined

Mualem (1976) developed a new theory for predicting the relative hydraulic conductivity [$K^r(\theta)$] from a soil water characteristic curve:

$$K^r(\theta) = S_e^{1/2} \left[\int_{\theta_r}^{\theta} \frac{1}{h(x)}dx \Big/ \int_{\theta_r}^{\theta_s} \frac{1}{h(x)}\,dx\right]^2 \qquad (2.34)$$

where

K^r = $K(\theta)/K^s$, relative hydraulic conductivity,

K^s = saturated hydraulic conductivity

$h(x)$ = soil water pressure head as a function of water content,

$S_e = \frac{\theta - \theta_r}{\theta_s - \theta_r}$, effective saturation

θ = water content,

θ_s = saturated water content,

θ_r = residual water content, value of porosity when water films lose effective continuity.

van Genuchten (1980) developed a closed form equation for predicting the hydraulic conductivity of unsaturated soil based upon Mualem's equation with the general retention equation of the form:

$$S_e = \left[\frac{1}{1 + (\alpha_1 h)^N}\right]^M \qquad (2.35)$$

where

h = absolute value of the pressure head,

α_1, N = nonlinear regression parameters to be determined, and

$M = 1 - 1/N$.

The relative hydraulic conductivity is expressed as a function of water content as:

$$K^r(\theta) = \left[\frac{\theta - \theta_r}{\theta_s - \theta_r}\right]^{1/2} \left\{1 - \left[1 - \left(\frac{\theta - \theta_r}{\theta_s - \theta_r}\right)^{1/M}\right]^{M}\right\}^2 \qquad (2.36)$$

Equations (2.35) and (2.36) do not consider hysteresis.

Stochastic Analysis

Soil is enormously heterogeneous. Nielsen et al. (1973) reported a wide range (four orders of magnitude) of steady state hydraulic conductivity in a 150 hectare experimental sire. They also reported the steady state hydraulic conductivities were log normally distributed (Nielsen et al., 1973). There is now a large body of direct evidence to support the statement that the probability density function for hydraulic conductivity is log normal. Law (1944) was the first to propose a log normal distribution on the basis of core analysis data from a carbonate oil field reservoir. Law's findings were supported by Bulnes (1946) and Warren et al. (1961). Willardson and Hurst (1965) found log normal distributions for the hydraulic conductivity of soil based on a study of 254 auger hole measurements in 12 fields in Australia and 1498 samples from seven soil types in California. Bennion and Griffiths (1966) worked with by far the largest sample of 60,000 cores from 2,000 wells in a sand and conglomerate oil field reservoir and 24,000 cores from 430 wells in a limestone reservoir. They found permeabilities to be log normal although in some cases somewhat skewed. Freeze (1975) reports, after careful examination of published data, that the values of standard deviation, σ, of the log saturated hydraulic conductivity lies between 0.2 and 2.0. But it is safe

(best) to assume that the variance in hydraulic conductivity distributions is independent of the mean values.

Considering the above facts, it is unwise to use a single value of K^S for solving groundwater flow problems, as is presently done in deterministic type solutions, especially since K^S is the most significant parameter in the groundwater flow equations. Using the mean value of K^S hides the uncertainty associated with such solutions. Thus, a stochastic model is much preferred. Stochastic models incorporate the randomness of the input and state variables, and their results are reported and interpreted in terms of means, variances, or standard deviations.

In a deterministic model, all mathematical and logical relationships between the elements are fixed. As a consequence, these relationships completely determine the solutions. In a stochastic model, at least one variable is random (Rubinstein, 1981).

The methods widely used for stochastic analysis of groundwater flow problems are the Monte Carlo method, spectral analysis technique, and perturbation techniques. McMillan (1966), Freeze (1975), Smith and Freeze (1979a,b), and Chung (1985) used the Monte Carlo method. Bennion and Hope (1974), Gelhar (1976), and Bakr et al. (1978) used the spectral analysis technique. Tang and Pinder (1977) used perturbation theory.

Monte Carlo method

The Monte Carlo method is a method of solving mathematical and physical problems approximately by simulation using random quantities or input variables (Chung, 1985). Because of the huge number of calculations

required, this method was not widely used before the appearance of electronic computers.

The use of the Monte Carlo method in stochastic groundwater problems involves repetitive simulations using a mathematical model coupled with a statistical analysis of the results. This method has been used quite extensively. Freeze (1975) used the Monte Carlo method for stochastic saturated flow studies without considering spatial correlation of soil properties. Smith (1978), and Smith and Freeze (1979a,b) considered spatial correlation in saturated hydraulic conductivity using a first order nearest neighbor model. Chung (1985) used the Monte Carlo method in modeling of water movement in the saturated-unsaturated zone. Hysteresis in the soil water retention and hydraulic conductivity was considered. The model considered layered geologic formations.

Monte Carlo techniques are used to solve the stochastic boundary value problems by repetitively solving a set of deterministic flow problems, each of which is an equally probable representation of the response of the real heterogeneous medium.

The random variable in a Monte Carlo model can be either discrete or continuous. Random numbers can be classified by pure random, pseudo-random, and quasirandom numbers. Generation of random numbers and transformation into a specific probabilistic distribution are discussed in many references (e.g., Rubinstein, 1981; Sobol, 1974; Hammersley and Handscomb, 1964). The Monte Carlo method has been used by others in groundwater studies (e.g., Smith and Hebbert, 1979; Warrick et al., 1977).

Groundwater Flow Models

Several types of models have been used to study groundwater flow systems. They are divided into three broad categories (Prickett, 1975): sand tank models, analog models (including viscous fluid models and electrical models), and mathematical models (including analytical and numerical models).

A model may be defined as a simplified version of the real (e.g., groundwater) system that approximately simulates the excitation-response relations of the latter (Bear and Verruijt, 1987). In simple words, we can say that a model is a tool designed to represent a simplified version of reality.

A sand tank model consists of a tank filled with an unconsolidated porous medium through which water is induced to flow. A field situation is scaled down to the dimensions of a laboratory model. Phenomena measured at the scale of a sand tank model are often different from conditions observed in the field, and conclusions drawn from such models may need to be qualified when translated to a field situation (Wang and Anderson, 1982).

Analog models are based on the fact that systems such as the flow of electrical current through a resistive medium or flow of heat through a solid, are analogous to the groundwater system.

A mathematical model of groundwater flow consists of a set of differential equations that are known to govern the flow of groundwater. Such models have been in use since the late 1800s. Simple assumptions are always made in order to construct a model because the field situations are too complex to be simulated exactly. A mathematical model consists of (i)

a definition of the geometry of the considered domain and its boundaries, (ii) an equation(s) that expresses the balance of the considered extensive quantity(ies), (iii) flux equations that relate the flux(es) of the considered extensive quantity(ies) to the relevant state variables of the problem, (iv) constitutive equations that define the behavior of the particular materials - fluids and solids - involved, (v) initial conditions that describe the known state of the considered system at some initial time, and (vi) boundary conditions that describe the interaction of the considered domain with its environment, across the boundaries of the former (Bear and Verruijt, 1987).

The preferable method of solution is the analytical one because once such a solution is derived, it can be used for a variety of situations. But in practice, this method is not feasible for most problems because of the complexities involved. So, numerical methods are used for solving the mathematical model. Often, the term numerical model is used instead of saying "numerical method of solution" (of the mathematical model).

Bear and Verruijt (1987) describe the main features of numerical models as:

1. The solution is sought for the numerical values of state variables only at specified points in the space and time domains defined for the problem (rather than their continuous variations in these domains).
2. The partial differential equations that represent balances of the considered extensive quantities are replaced by a set of algebraic equations written in terms of the sought, discrete values

of the state variables at the discrete points in space and time mentioned in (1).

3. The solution is obtained for a specified set of numerical values of the various model coefficients (rather than as general relationships in terms of these coefficients).
4. Because of the very large number of equations that have to be solved simultaneously, a computer code has to be prepared in order to obtain a solution, using a digital computer.

The governing equation of saturated-unsaturated flow is a nonlinear (equation 2.11) partial differential equation with variable coefficients. Numerical methods are the best ways to the solution of such flow problems. In recent years, the two most widely used numerical solutions methods are the finite difference method and the finite element method. Each one has its own advantages and disadvantages, and it is hard to say that one is always better than the other. It depends on the problem being modeled and other conditions (Chung, 1985). These two approximate methods provide a rationale for operating on the differential equations that make up a model and for transforming them into a set of algebraic equations. Before digital computers were widely available, only hand calculations were possible and these techniques were of limited value. A numerical solution can be tested by comparing it with an analytical solution, if one is available, or the solution can be checked with the values observed in the field. The procedure is summarized in Figure 2.8.

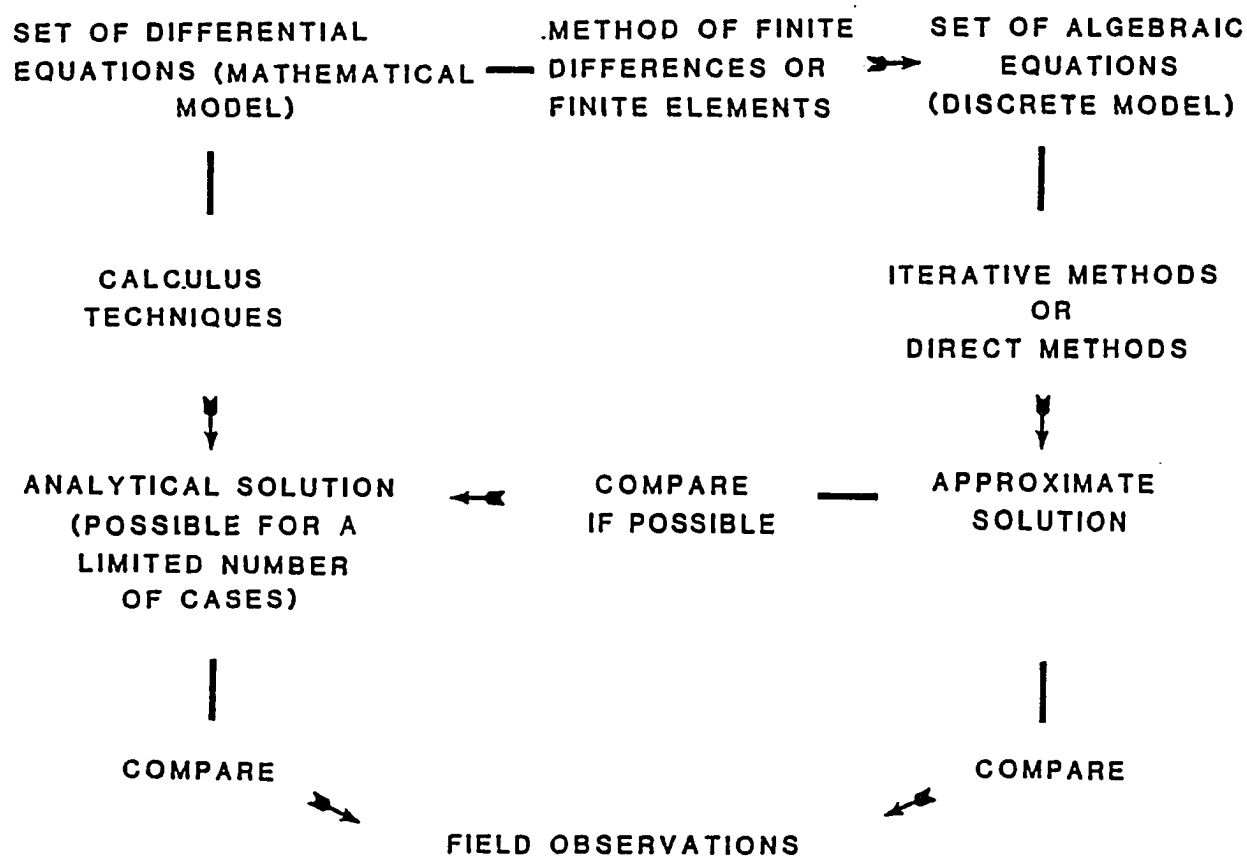

Figure 2.8. Relationship between mathematical model, discrete algebraic model, analytical solution, approximate solution, and field observations (Wang and Anderson, 1982)

Finite difference method

In the finite difference method, all derivatives are replaced by finite differences and thus reduce the original continuous boundary value problem to a discrete set of simultaneous algebraic equations. If there are N nodes, there are N finite-difference equations which are linear. There are also N unknowns - say the N values of h (pressure head) at the N nodes. Now it is possible through various techniques to solve these N equations to find N unknowns. Detailed descriptions on the finite difference method are available in many publications (e.g., Richtmyer and Morton, 1967; Remson et al., 1971; Lapidus and Pinder, 1982; Wang and Anderson, 1982; and Bear and Verruijt, 1987).

Finite element method

A second very powerful method is the finite element method. In groundwater flow problems, one could imagine that a region is subdivided into small elements, such that for each element the flow is described in terms of the head at the nodal points and then a system of equations is obtained from the condition that the flow must be continuous at each node.

The application of the finite element method to groundwater problem is a relatively recent development compared with the finite difference method.

Proponents of the finite element method point to its flexibility for problems in which the boundaries are irregular or for problems in which the medium is heterogeneous or anisotropic. The finite difference method can also account for these complications. However, the flexibility of the finite element method is useful in solving coupled problems, such as

contaminant transport, or in solving moving boundary problems, such as a moving water table (Wang and Anderson, 1982).

The concept of elements (that is, the subareas delineated by the lines connecting nodal points) is fundamental to the development of equations in the finite element method. Elements can be of different shapes. In groundwater flow problems, the nodes are the points within the problem domain at which the heads are to be computed. Furthermore, the head within each element is defined in terms of the nodal values by a basis or interpolation function. The use of an interpolation function to define the potential throughout the problem domain is an important concept that distinguishes the finite element method from the finite difference method. In the finite difference method, the head is defined only at the nodal points themselves. The definition of the head throughout the problem domain in the finite element method permits the application of variational or weighted residual principles.

The philosophy behind the variational principle is that a physical quantity, such as the rate of energy dissipation, be minimized over the problem domain. This rate can be expressed in terms of the potential (head) throughout the domain. If the potential is expressed in terms of its nodal values, the variational principle leads to algebraic equations.

A weighted residual principle is expressed in terms of the governing partial differential equation without need to resort to a physical quantity. The residual at each point in the problem domain is a measure of the degree to which the head does not satisfy the governing equation. If a

particular weighted average of the residual is forced to vanish, the nodal heads are obtained as the solution of a system of algebraic equations.

The finite element method combines several mathematical concepts to produce a system of linear or nonlinear equations. The method is easily applied to irregular shaped objects composed of several different materials and having mixed boundary conditions.

The finite element method can be subdivided into five basic steps (Segerlind, 1984). They are:

1. Discretize the region. This includes locating and numbering the node points, as well as specifying their coordinate values.
2. Specify the approximation equation. The order of the approximation, linear or quadratic, must be specified and the equations must be written in terms of the unknown nodal values. An equation is written for each element.
3. Develop the system of equations. When using Galerkin's method, the weighting function for each unknown nodal value is defined and the weighted residual integral is evaluated. This generates one equation for each unknown nodal value. In the potential energy formulation, the potential energy of the system is written in terms of the nodal displacements and then is minimized. This gives one equation for each of the unknown displacements.
4. Solve the system of equations.
5. Calculate quantities of interest.

The finite element method has two characteristics that distinguish it from other numerical procedures:

1. The method utilizes an integral formulation to generate a system of algebraic equations.
2. The method uses continuous piecewise smooth functions for approximating the unknown quantity(ies).

It is applicable to steady-state and time-dependent problems as well as problems involving nonlinear material properties. General computer programs that are user-independent can be, and have been, developed.

The choice of whether a finite element method or finite difference method is better depends on variables such as:

1. complexity of the flow system,
2. computer time required for solution,
3. problems of stability and truncation error, and
4. applicability of computer programs (Todd, 1980).

CHAPTER 3. MODEL DEVELOPMENT

In the present study, a finite element model has been developed to predict:

1. the pressure head and water content at different depths,
2. water table elevation,
3. tile outflow,
4. evaporation and transpiration rate,
5. infiltration, and
6. deep percolation under transient field conditions in a two-dimensional saturated-unsaturated soil profile.

The Monte Carlo method is used to simulate a large number of equally probable values of saturated hydraulic conductivity, which are generated from a log-normal distribution that can be used as inputs to the model. The results from the Monte Carlo simulations are analyzed using standard statistical routines.

In the development of this model, the following considerations were made:

1. required input data should be easily available,
2. the model should be easy to modify,
3. stochastic nature of the saturated hydraulic conductivity should be preserved,
4. the model should be able to handle the presence of more than one non-homogeneous layered geologic formation.

Assumptions

The following are the main assumptions made in the development of this model:

1. the flow system is considered continuous throughout the saturated-unsaturated zone;

2. Darcy's Law is valid for describing water flow, i.e., the flow is laminar;

3. no water quality variable or electrochemical effects are considered;

4. the effects of temperature gradients, osmotic gradients and other minor gradients on water flow are disregarded;

5. water vapor transport is not considered;

6. the effect of temperature on the hydraulic conductivity is neglected;

7. hysteresis is not considered; and

8. only hydraulic conductivity of the soil water is considered stochastic.

Finite Element Equation

A finite element solution of equation (2.11) has been presented by Neuman and Davis (1983). They used the Galerkin finite element method using triangular elements (when rectangular elements are used, the program automatically divides the rectangular elements into two triangular elements) in deriving the solution.

The basic equations are as follows:

$$\sum_{m=1}^{N} A_{nm} h_m + \sum_{m=1}^{N} F_{nm} \frac{dh_m}{dt} = Q_n - B_n - D_n, \quad n = 1,2,\ldots N \tag{3.1}$$

for a vertical cross section described by the coordinates x (horizontal) and z (vertical) where N = total number of nodes

$$A_{nm} = \sum_{e} \frac{1}{4\Delta} \bar{K}^r \left(K^s_x b_n b_m + K^s_z c_n c_m\right)$$

$$F_{nm} = \sum_{e} \frac{\Delta}{12} \left(2C_n + C_p + C_q\right) + 4\beta S_s \text{ if } n = m$$

$$= 0 \text{ if } n \neq m$$

$$Q_n = -\sum_e \frac{(LV)_n}{2}$$

$$B_n = \sum \frac{1}{2} \bar{K}^r \, (K^s_z \, c_n),$$

where

D_n = root uptake of water at node n,

Δ = area of the triangular element,

n, p, q = nodes of the triangle,

$\bar{K}^r$ = average relative hydraulic conductivity,

$= (K^r_n + K^r_p + K^r_q)/3$,

b, c = geometric coefficients (see Appendix A),

L = length (includes the nodes at the end),

V = infiltration or evaporation rate,

K^s_x = saturated horizontal hydraulic conductivity,

K^s_z = saturated vertical hydraulic conductivity,

C = specific moisture capacity,

h_m = pressure head at node m, m = 1, 2, ... N, and

β, S_s have been defined earlier.

Some observations about the above equation:

1. Matrix A_{nm} is sparse and symmetric.
2. Matrix F_{nm} is diagonal.
3. At all internal nodes which do not act as sources or sinks, elements of vector Q_n are zero.
4. Vector B_n accounts for gravity and thus its elements will be zero in the case of horizontal flow.

5. The effect of water withdrawal by plant roots are represented by vector D_n.

In deriving equation (3.1), it was assumed that saturated hydraulic conductivities remain constant while relative conductivity, K^r, and specific moisture capacity, C, are assumed to vary linearly according to:

$$K^r = K_p^r N_p^e \tag{3.2}$$

$$C = C_p N_p^e \tag{3.3}$$

where

p = corners of the triangle, and

N_p^e = local coordinate function associated with node p in element e.

Integration of equation (3.1) is achieved by discretizing the time domain into a sequence of finite intervals and replacing the time derivatives by finite differences.

A fully implicit backward difference scheme, in terms of h, is:

$$\left(A_{nm}^{k+\frac{1}{2}} + \frac{1}{\Delta t^k} F_{nm}^{k+\frac{1}{2}}\right) h_m^{k+1}$$

$$= Q_n^{k+\frac{1}{2}} - B_n^{k+\frac{1}{2}} - D_n^{k+\frac{1}{2}} + \frac{1}{\Delta t^k} F_{nm}^{k+\frac{1}{2}} h_m^k \tag{3.4}$$

where

k represents the time $t=t^k$, and $\Delta t^k = t^{k+1} - t^k$.

Evaluation of the coefficients in equation (3.4) requires that pressure heads be known at the middle of each time step. A first estimate of these heads is obtained by linear extrapolation of previously calculated values:

$$h_n^{k+\frac{1}{2}} = h_n^k + \frac{\Delta t^k}{2\Delta t^{k-1}} \left(h_n^k - h_n^{k-1}\right) \tag{3.5}$$

The resulting set of simultaneous linear algebraic equations are then solved for the values of pressure head at all nodes at time t^{k+1} by Gaussian elimination. An iterative process is used to improve these results until a satisfactory degree of convergence is obtained for the time step. At each iteration, the most recent values of pressure head are averaged with the results from the last time step to obtain improved estimates of the current time step:

$$h_n^{k+\frac{1}{2}} = \frac{1}{2} (h_n^k + h_n^{k+1}), \quad n = 1,2,\ldots,N \tag{3.6}$$

The coefficients are then reevaluated with equation (3.4) and the new equations are again solved by the Gaussian elimination.

Initial Conditions

To solve the finite element equations, it is necessary to know the initial conditions within the flow region. Initial conditions are the known pressure heads at the nodes at time zero. Thus, the pressure heads must be known at all nodes within the domain at the beginning of the simulation.

Boundary Conditions

The boundary conditions can be of several types:

1. prescribed head,
2. prescribed flux,
3. root zone,
4. evaporation,
5. infiltration,
6. seepage,

7. impermeable, and

8. sink/source.

Prescribed head boundary

Suppose that the value of pressure head at some node p must be equal to a prescribed value hp at the end of Δt^k. Instead of eliminating the equation for the pth node, it is replaced by the dummy expression:

$$A_{pp}\ h_p^{k+1} = h_p \qquad (3.7)$$

where

$$A_{pp} = 1$$

The values of h^{k+1} in all other equations are simply set equal to hp and moved to the right hand side in order to preserve matrix symmetry. After solving for all pressure heads, the value of Q_p can be calculated explicitly from the original finite element equation for node p.

Prescribed flux boundary

The known values of Q_n are used to write the equation for node n according to equation (3.4).

Root zone

The root zone must consist only of rectangular elements with boundaries parallel to the coordinate axes. Either the Neuman and Davis (1983) model or the Molz and Remson (1970) model can be used, as described below.

Neuman and Davis (1983) model

A root zone is shown in Figure 3.1. By assuming that root extraction rate varies linearly in the vertical direction between two adjacent nodes, the root extraction term (D_n) at node n is:

$$D_n = \frac{(W_{i-1} + W_i)}{2} \sum_{L} L \left(\frac{S_n}{3} + \frac{S_{n+1}}{6}\right) \quad (3.8)$$

where,

W_i = distance between nodal columns i and i+1,

S_n = root uptake at node n, and

L = vertical distance between adjacent nodes along a nodal column.

Neuman defines S as

$$S = K^r K^s_x (h - h_r) b' \ldots \quad (3.9)$$

where,

h_r = pressure head in the plant roots,

b' = root effectiveness function, and

K^r and K^s_x have been defined earlier.

The root effectiveness function is dependent on depth and time. Neuman and Davis (1983) treat it as an empirical quantity that should be determined experimentally. Feddes et al. (1978), Nimah and Hanks (1973), and Gardner (1964) have more information on root effectiveness function, b'.

Substituting equation (3.9) into equation (3.8) leads to:

$$D_n = \frac{(W_{i-1} + W_i)}{2} \sum_{L} L K^s_x \left(\frac{[K^r b' (h-h_r)]_n}{3} + \frac{[K^r b' (h-h_r)]_{n+1}}{6}\right) \quad (3.10)$$

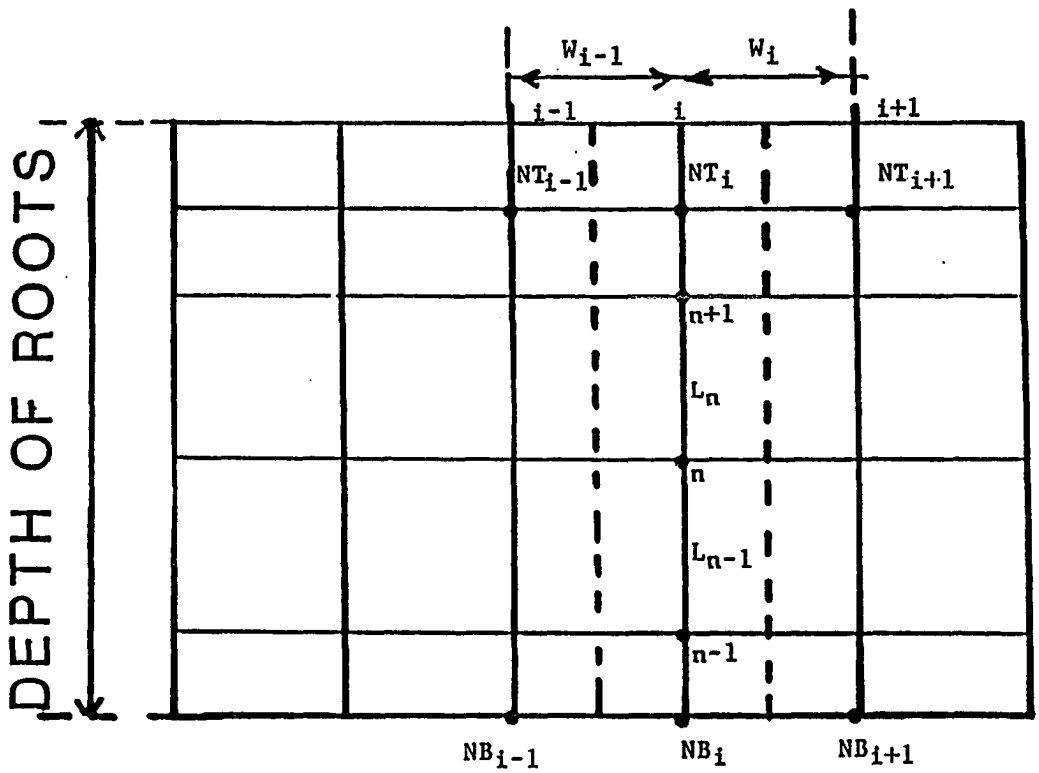

Figure 3.1. Rectangular nodal pattern in root zone (Neuman and Davis, 1983)

where,

h_r is assumed to remain uniform with depth.

The total rate of transpiration per unit surface area is given by:

$$T = \frac{2}{W_{i-1} + W_i} \sum_{n=NB_i}^{NT_i} D_n \quad , \quad D_n<0 \tag{3.11}$$

where,

T = rate of transpiration,

NB_i = bottom node in ith column, and

NT_i = top node in ith column of root zone.

The actual rate of root extraction is obtained by maximizing equation (3.11) subject to:

$$| T | \leq | PT |$$

and $h_r \geq h_w$

where,

PT = potential rate of transpiration, and

h_w = wilting point pressure head.

This process is outlined in the following

1. h_r is set equal to the prescribed value of h_w.
2. Using prior values of $h^{k+\frac{1}{2}}$ and $(K^r)^{k+\frac{1}{2}}$, the value of $D_n^{K+\frac{1}{2}}$ is calculated for each node in the column with equation (3.10).
3. Setting positive values of D_n to zero, T is calculated with equation (3.11).
4. If | T | is less than or equal to | PT |, the values of D_n as calculated in 2 above are utilized in the solution of equation (3.4).
5. If | T | is greater than | PT |, all values of D_n as calculated in 2 above are multiplied by the quantity | PT |/| T | so as to make their sum equal to | PT |.

Molz and Remson (1970) model

This model is based on an empirical rule used by some agricultural workers to approximate the extraction pattern of plant roots. The model assumes that 40%, 30%, 20%, and 10% of the total transpiration requirement comes from each successively deeper quarter of the root zone, respectively. An extraction term that meets the above percentage requirement is

$$S(Z) = -\frac{1.6\,T}{V^2} Z + \frac{1.8\,T}{V} \qquad 0 \le Z \le V \tag{3.12}$$

where,

S (Z) = the moisture extraction rate per unit volume of soil, cm,

Z = soil depth from which root extraction occurs, cm,

V = total root zone depth, cm, and

T = total transpiration, cm.

The total moisture extraction rate from a volume of soil of unit cross section bounded by the horizontal planes $Z = Z_1$, and $Z = Z_2$ where $Z_1 < Z_2$ is

$$\int_{Z_1}^{Z_2} S(Z)\,dZ = \frac{-1.6T}{V^2} \frac{Z^2}{2}\Bigg|_{Z_1}^{Z_2} + \frac{1.8T\,Z}{V}\Bigg|_{Z_1}^{Z_2} \quad \ldots \tag{3.13}$$

Equation (3.13) is used to distribute potential transpiration in this model. Using equation 3.13, the potential transpiration rate is calculated for different sublayers. The potential transpiration for each node in that layer is assigned based on the horizontal width each node represents.

Evaporation/infiltration boundary

These boundaries are simulated by applying either prescribed head or prescribed flux boundaries. The governing equation for flux normal to the boundary is represented mathematically by:

$$[K^r K^s_x \frac{\partial h}{\partial x}] n_x + [K^r(K^s_z \frac{\partial h}{\partial z} + K^s_z)] n_z = -V(x, z, t) \quad (3.14)$$

where n_x and n_z are the x-th and z-th components of a vector of unit length normal to the boundary and pointing outward and V (flux) is a prescribed function of (x, z, t). K^s_x denotes horizontal saturated hydraulic conductivity and K^s_z is the vertical saturated hydraulic conductivity. The actual evaporation or infiltration is obtained by maximizing the absolute value of the flux (while maintaining the appropriate sign) subject to the following requirements.

$$[K^r K^s_x \frac{\partial h}{\partial x}] n_x + [K^r (K^s_z \frac{\partial h}{\partial z} + K^s_z)] n_z \leq E_s^* \quad (3.15)$$

and $h_L \leq h \leq 0$ (3.16)

where

E^*_s = prescribed potential surface flux, and

h_L = minimum allowed pressure head at the soil surface.

Potential surface flux is a function of time. It should be noted that potential surface flux is positive for infiltration situation and negative for evaporation situation. The potential surface flux value should be provided as an input. During the first iteration of any time step, such nodes are treated as prescribed flux boundaries with a flux equal to some fraction of the specified potential flux. If computed pressure head values

satisfy equation (3.16), the absolute value of the flux at the node is increased by an amount calculated according to:

$\frac{|h_L|}{|h_n|}$ in the case of an evaporation boundary

$\frac{|h_L|}{|h_L - h_n|}$ in the case of an infiltration boundary

But the increased value must not exceed the potential flux value. If, however, equation (3.16) is not satisfied, node n becomes a prescribed head boundary during subsequent iterations with:

$h = h_L$ for evaporation boundaries, and

$h = 0$ for infiltration boundaries.

When actual infiltration rate is less than potential infiltration rate, there will be storage on top of the surface. For such conditions, the nodes will be treated as prescribed head nodes with a head equal to the height of stored water. The stored water is allowed time to infiltrate until all the water is infiltrated or evaporated.

Seepage boundary

The nodes through which seepage can occur are identified and at each iteration they are checked to see whether they are saturated or unsaturated. If a seepage node is saturated, the node is treated as a prescribed pressure head boundary with h=0. At the same time, the unsaturated nodes are treated as a prescribed flux boundary with Q=0.

Impermeable boundary

The impermeable nodes have zero flux boundary conditions.

Sink/source boundary

The known values of Q for such nodes is to be assigned.

Other Model Components

Surface runoff

Surface runoff is calculated by the Mockus (1972) curve number technique. This method was selected because required inputs are generally available and it relates runoff with soil type, land use, and management practices. Runoff is predicted by using the Soil Conservation Service (SCS) equation.

$$Q = \frac{(P - 0.2S)^2}{P + 0.8S} \tag{3.17}$$

where:

Q = actual runoff, inches,

P = cumulative rainfall, inches, and

S = retention parameter, inches.

S is estimated by using the equation:

$$S = \frac{1,000}{CN} - 10 \tag{3.18}$$

where:

CN = curve number based on an antecedent moisture condition (AMC) determined by the total rainfall in the 5-day period preceding a storm.

The Curve Number (CN) can be obtained for various land use, treatment or practice, hydraulic conditions, soil group, and antecedent moisture

conditions from standard hydrology textbooks or manuals (e.g., Mockus, 1972).

Interception

In this model, the maximum potential interception storage was determined as a linear function of crop leaf area index (CLAI) for CLAI less than or equal to 3.0 following Anderson (1975):

$$INTCEP = 0.038 * CLAI \quad (3.19)$$

where,

INTCEP = potential interception in cm.

Figure 3.2 shows the relationship between CLAI and the growing period.

Potential evapotranspiration

The potential evapotranspiration rate is calculated either by using the modified Penman method or by using Shaw's method. Both of these methods have been discussed in the literature review chapter. The hourly distribution of daily potential evapotranspiration is assumed following Anderson (1975) as follows:

Midnight to 4:00 a.m.	:	2.4% of daily PET
4:00 a.m. to 8:00 a.m.	:	4.8%
8:00 a.m. to 12:00 noon	:	29.0%
12:00 noon to 4:00 p.m.	:	39.7%
4:00 p.m. to 8:00 p.m.	:	19.5%
8:00 p.m. to midnight	:	4.6%

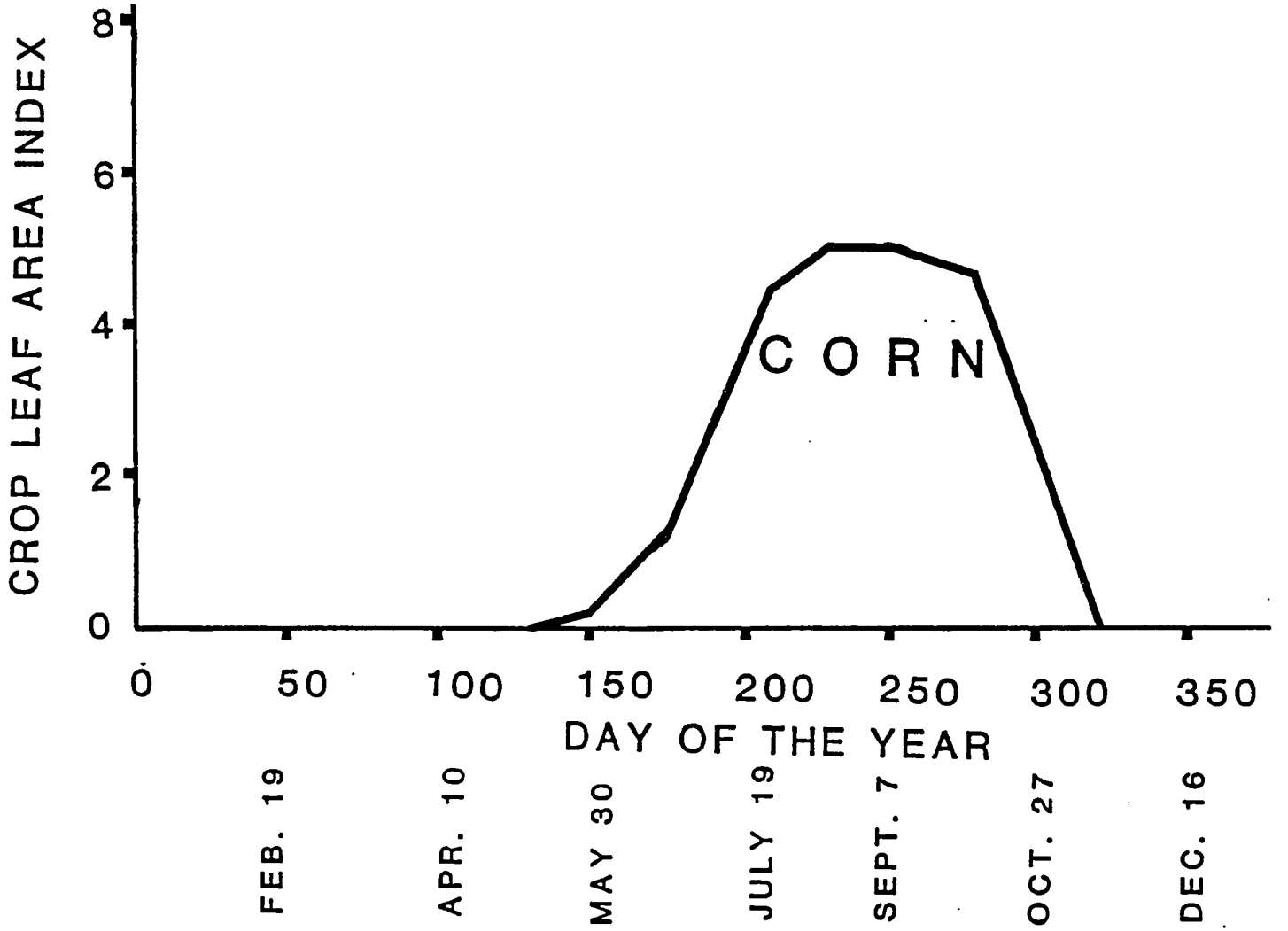

Figure 3.2. CLAI curve for corn (Anderson, 1975)

Division of PET into PE and PT

The model requires that potential evaporation and potential transpiration data be provided as separate input values. The potential evaporation from bare soil surfaces may be estimated by various methods, including the following equation:

$$PE = \frac{\delta/\gamma}{(\delta/\gamma+1)L} R_n \exp\,[-0.39\ (CLAI)] \qquad (3.20)$$

where:

PE = potential evaporation,

δ = slope of saturation vapor pressure curve,

γ = psychrometric constant,

L = latent heat of water vaporization,

R_n = net radiation flux, and

CLAI = crop leaf area index.

PT (potential transpiration) is obtained from subtracting the PE value (Eq. 3.20) from PET (Eq. 2.12).

$$PT = PET - PE$$

It may not be possible to have all the necessary data to use equations (2.12) and (3.20) in most cases. When PET is calculated using only pan evaporation data, there is no reliable method to separate PET into PE and PT. Some field experiments have been reported (e.g., Tanner, 1960; Peters and Russell, 1959; Harrold et al., 1959; Fritschen and Shaw, 1961) that show the ratio between soil evaporation and transpiration will vary with the type and amount of crop cover. Early in the season, all loss is by

soil evaporation. As the crop cover increases, both evaporation and transpiration occur. As the crop grows in size and gives a more complete ground cover, the evaporation is lowered and transpiration is increased. Even in experimental plots, it is extremely difficult to separate evaporation and transpiration. In this model, an attempt has been made to separate PET into PE and PT based on information available on CLAI and the fraction of crop canopy which is actively transpiring at any time during the growing season (Table 3.1). Figures 3.2 and 3.3 provide information on CLAI and fraction of the plant canopy actively transpiring of corn. Table 3.1 should be changed when the crop is different.

Actual evaporation

The way this model calculates actual evaporation from given potential evaporation has been discussed earlier in this section.

Actual transpiration

If the Neuman and Davis (1983) model of root water uptake is used, the root effectiveness ratio plays an important role other than available moisture content in determining actual transpiration. This process was described earlier in the chapter. If the Molz and Remson (1970) model is used, the actual transpiration is calculated based on the assumption that the roots will not be able to transpire any water at wilting point, but they will transpire at potential rate at midpoint between wilting point and field capacity (water content at -1/3 bar pressure). Between these two points, the relationship between actual and potential transpiration is linear. Figure 3.4 shows this relationship.

Table 3.1. Separation of PET into PE and PT for corn

Period			Fraction of plant canopy actively transpiring	% of PET	
Days of the year	Dates	CLAI		PE	PT
130-139	05/10-05/19	0.1	1.0	100	0
140-149	05/20-05/29	0.2	1.0	95	5
150-159	05/30-06/08	0.6	1.0	90	10
160-169	06/09-06/18	1.0	1.0	80	20
170-179	06/19-06/28	1.5	1.0	70	30
180-189	06/29-07/08	2.5	1.0	50	50
190-199	07/09-07/18	3.5	1.0	30	70
200-209	07/19-07/28	4.5	1.0	10	90
210-219	07/29-08/07	4.75	1.0	10	90
220-229	08/08-08/17	5.0	0.9	10	90
230-239	08/19-08/27	4.8	0.8	20	80
240-249	08/28-09/06	4.6	0.65	35	65

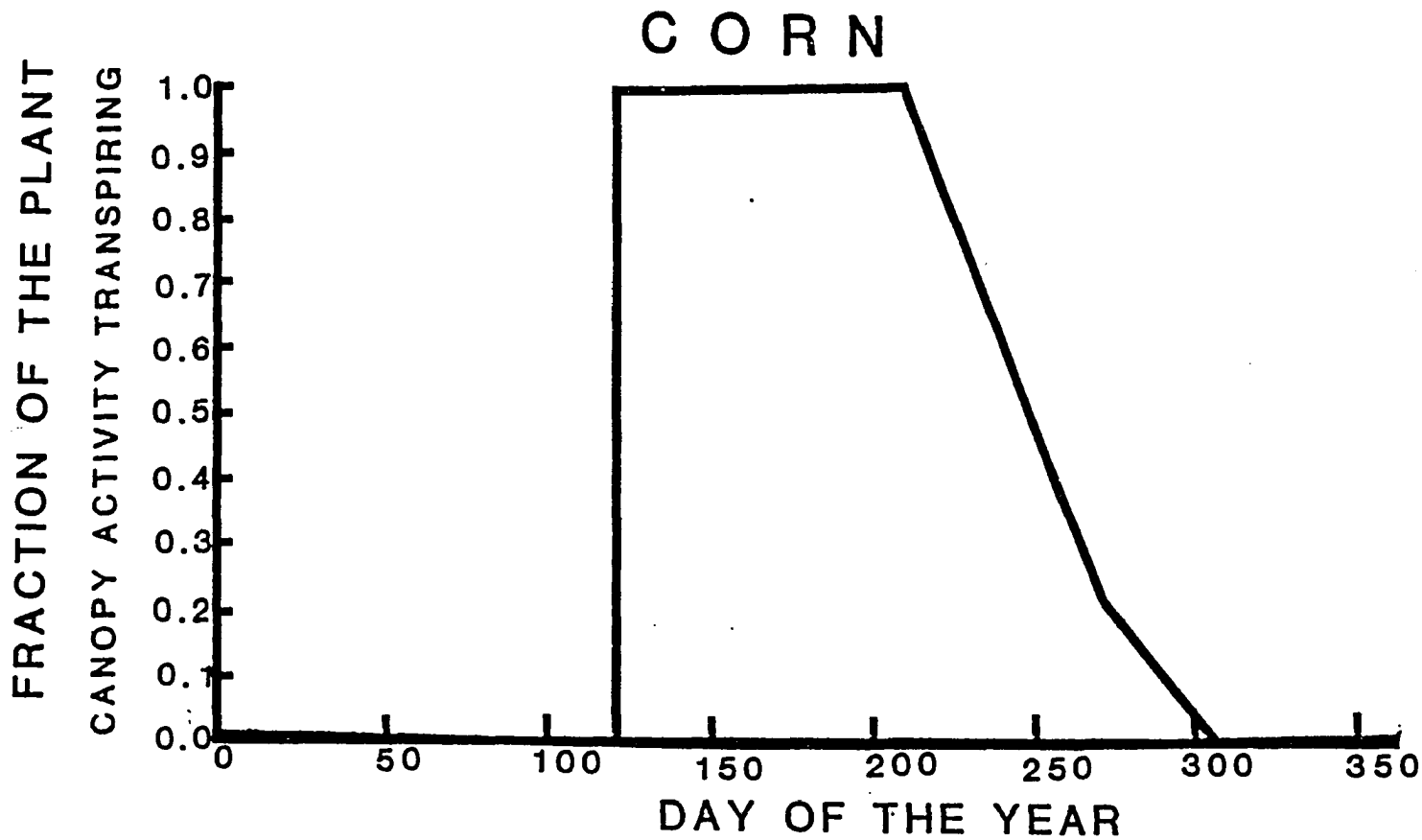

Figure 3.3. Curve showing the decimal fraction of corn canopy which is actively transpiring (Anderson, 1975)

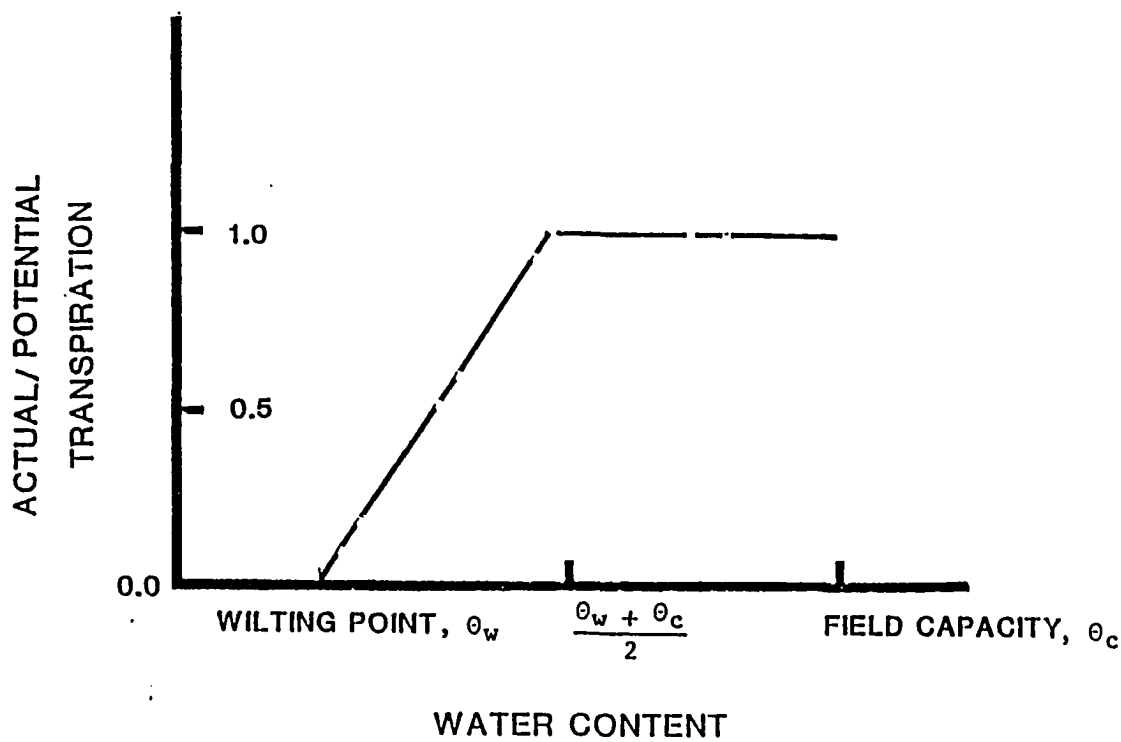

Figure 3.4. Relation used to calculate actual transpiration (Chung, 1985)

Soil-moisture characteristic curve

Information on the water content-pressure head relationship must be provided as an input for functioning of the model. The determination of the water content-pressure head relationship of a soil can be done either from field or laboratory measurements. For the field determination, several tensiometers at various depths and a neutron probe can be used for the pressure head and moisture content measurement, respectively. By this method, it may take quite some time to construct a well-defined soil moisture characteristics curve.

Laboratory determination of the water content-pressure head relationship has been extensively used. A tension table or pressure funnel is used for creating low levels of tension and a pressure chamber is used for creating high tensions (e.g., 1 bar to 20 bars).

In this model, hysteresis has been ignored. For this reason, only the drying curve is used which is measured by gradually extracting water from an initially saturated soil sample. This method is also known as the desorption method.

Determination of specific moisture capacity

Specific moisture capacity as a function of water content is determined from the slope of the soil moisture characteristic curve by linear interpolation. For example, from the soil moisture characteristic curve, the following values were obtained:

at $\theta_1 = 0.028$, $h_1 = -200.00$ cm

$\theta_2 = 0.062$, $h_2 = -100.00$ cm

$$\text{so at } \theta_{ave} = \frac{0.028 + 0.062}{2} = 0.045,\ C = \frac{d\theta}{dh} = \frac{0.028 - 0.062}{-200 - (-100)} = 0.0034$$

where

C = specific moisture capacity.

Repeating this procedure for different θ's gives the specific moisture capacity versus water content relationship.

Hydraulic conductivity

The model requires both saturated vertical and horizontal hydraulic conductivity as input. Field measurements should be the most preferable choice. It may not be possible to measure these values in the field (especially at deeper depths) because of unavailability of reliable instruments. Laboratory measurements thus become necessary. Undisturbed soil samples are brought to the laboratory and saturated hydraulic conductivity can be measured by various methods following standard procedures. The saturated hydraulic conductivity measured in the laboratory is the vertical one. The horizontal hydraulic conductivity is sometimes assumed as a multiple (e.g., 4 to 5 times) of vertical hydraulic conductivity.

Unsaturated hydraulic conductivity

It is obvious from an examination of equation (2.11) that information on unsaturated hydraulic conductivity is necessary to analyze soil moisture movement in the unsaturated zone. The method developed by van Genuchten (1980) based on Mualem's (1976) theory is used for predicting the relative hydraulic conductivity ($K^r(\theta)$) as a function of water content. Following

this method, the soil moisture retention data (characteristics curve) are fitted to the following equation by the nonlinear regression technique.

$$\theta = \theta_r + (\theta_s - \theta_r) \left[\frac{1}{1 + (\alpha_1 h)^N}\right]^M \tag{3.21}$$

where:

θ = water content,

θ_r = residual water content,

θ_s = saturated water content,

h = absolute value of pressure head,

α_1,N = regression parameters, and

M = 1 - 1/N

The fitted θ_r, M values are then used in the following equation to predict relative hydraulic conductivity as a function of water content.

$$K^r(\theta) = \left[\frac{\theta - \theta_r}{\theta_s - \theta_r}\right]^{1/2} \left\{1 - \left[1 - \left(\frac{\theta - \theta_r}{\theta_s - \theta_r}\right)^{1/M}\right]^M\right\}^2 \tag{3.22}$$

where:

$$K^r(\theta) = \frac{K(\theta)}{K^s}$$

Stochastic Analysis

The Monte Carlo method of stochastic analysis has been used in this study. As explained earlier, the Monte Carlo method involves the repetition of a number of simulations. In each Monte Carlo run, a different set of saturated hydraulic conductivities for all the layers was

used. The model used for generating the saturated hydraulic conductivities is explained below.

The model

Saturated hydraulic conductivity is assumed to be log normally distributed. If we define Y = ln K, then it is assumed that Y is normally distributed. Conductivity realizations are generated with the normal generator

$$Y = \sigma R_N + \mu_y \tag{3.23}$$

where:

R_N = a random number taken from N[0,1],

σ = standard deviation of saturated hydraulic conductivity,

μ_y = mean value of saturated hydraulic conductivity.

Since Y = ln K, the log normal generator for K^S is

$$K^S = \exp\ [(\sigma\ R_N + \mu_y)] \tag{3.24}$$

In the present study, the soil profile was divided into four layers based on field observations. Mean saturated hydraulic conductivity and standard deviation of K^S was calculated by taking out undisturbed soil samples from these four layers and measuring K^S in the laboratory. To preserve the mean tendency of the saturated hydraulic conductivity in the profile, the four K^S values in each Monte Carlo run was realized by using the same random number generated in that run. Thus, in any Monte Carlo run:

$$K^{s1} = \exp\left[\sigma_1 R_N + \mu_{y1}\right] \tag{3.25}$$

$$K^{s2} = \exp\left[\sigma_2 R_N + \mu_{y2}\right] \tag{3.26}$$

$$K^{s3} = \exp\left[\sigma_3 R_N + \mu_{y3}\right] \tag{3.27}$$

$$K^{s4} = \exp\left[\sigma_4 R_N + \mu_{y4}\right] \tag{3.28}$$

where the subscripts 1, 2, 3, and 4 refer to layers. In the program, these K^s values are used as saturated vertical hydraulic conductivity ($K^s{}_z$) values.

CHAPTER 4. FIELD AND LABORATORY MEASUREMENTS

The experimental area was located at the Agronomy-Agricultural Engineering Research Center, five miles west of Ames in central Iowa. The study site has six plots, each with a single tile drain. A profile with 18.29 m width and 1.83 m depth with a single tile at 1.22 m depth was used for this research. The major soil type at the study site was Clarion loam soil (fine loamy, mixed, mesic type hapludolls) of the Clarion-Nicollet-Webster Soil Association with a maximum slope of 2%. Corn and soybeans are the major crops. In 1987, corn was grown. The particular plot used for research is in no-till cultivation. The mean bulk-density, porosity, pH, organic matter content, and particle sizes of the soil at the experimental site is given in Tables 4.1 and 4.2.

In the no-tillage system, there is no turning and loosening of the soil material with tillage. Plant residues are left on the soil surface where they form a mulch cover. The only disturbance in the soil is due to planting and cultivation in such a no-tillage systems.

Based on field observations, the 122 cm soil profile was divided into four layers for collecting soil samples. The layers were 0-15.0 cm, 15.0-30.5 cm, 30.5-61.0 cm, and 61.0-122.0 cm. No samples were collected between 122.0-183.0 cm. This portion was considered to have the same properties as the layer of 61.0-122.0 cm.

The tiles were 10.2 cm in diameter and spaced 36.6 m apart. To provide access to the subsurface tile lines, 1.5 m deep sumps were dug to intercept the drain tiles. The entrance tile emptied into a collection tank equipped with either a small H-flume or a V-notch weir for a flow

Table 4.1. Soil properties of the experimental plot

Layer	Depth (cm)	Mean bulk density (gm/cm^3)	Porosity	pH	Organic Content
1	0.0- 15.0	1.515	0.4282	5.0	2.49
2	15.0- 30.5	1.388	0.4763	5.4	2.36
3	30.5- 61.0	1.405	0.4697	5.9	1.87
4	61.0-122.0	1.486	0.4392	6.2	0.96

Table 4.2. Particle size distribution of soil of the experimental plot

Layer	Depth (cm)	Sand (%)	Coarse Silt (%)	Fine Silt (%)	Clay (%)
1	0.0- 15.0	42.0	16.3	18.8	22.9
2	15.0- 30.5	35.7	16.8	21.4	26.1
3	30.5- 61.0	34.1	16.5	21.8	27.6
4	61.0-122.0	45.5	13.4	17.1	24.0

measuring device. A float-activated continuous water stage recorder was used in conjunction with either the flume or weir to provide a record of tile flow rates as a function of time. Three observation wells (1.8 m long, 33 mm diameter plastic pipe with open bottom and perforated sides) were installed in each plot midway between the subsurface drains and were used to measure the water table fluctuations in each plot.

Field Measurements

Field measurements included pressure head at 15.0 cm, 30.5 cm, 61.0 cm, 91.0 cm, and 122.0 cm depths, water table elevation and tile flow rate (Appendix B). A portable pressure transducer was used to measure the moisture tension (pressure head) in the tensiometer. Tensiometer readings during very dry periods near the surface were not used as they were not reliable. Precipitation (hourly) and open pan evaporation data were collected from National Oceanic and Atmospheric Administration Publications (Station: Ames 8 WSW).

Laboratory Measurements

The laboratory measurements included dry bulk density, saturated hydraulic conductivity, water content of the soil samples taken at the surface, organic content, clay, sand, and silt content, pH, and soil water retention. The laboratory values of saturated hydraulic conductivity were used as the vertical saturated hydraulic conductivity in the model. Horizontal saturated hydraulic conductivity was assumed to be five times (two times in one simulation) higher than vertical saturated hydraulic conductivity.

Saturated hydraulic conductivity

The constant head method was used in measuring saturated hydraulic conductivity. In this method, a constant head is created on the top surface of the completely saturated soil sample. Outflow rate is measured and Darcy's equation is solved to find out saturated hydraulic conductivity.

Darcy's equation is:

$$K = \left(\frac{Q}{A\ t}\right) L/H \qquad (4.1)$$

where

K = hydraulic conductivity,

Q = volume of outflow,

A = cross-sectional area of cylinder (soil sample),

H = hydraulic head,

L = soil column length, and

t = time required to collect Q.

Table 4.3 provides information on laboratory measurements of saturated hydraulic conductivity. Some samples collected were not used because some of them had cracks and holes and some were compactred during the process of collecting the samples.

Soil-moisture characteristic curve

Soil water retention data (for the drying curve) for the four layers were determined using both a pressure funnel and a pressure plate (Appendix B). In the pressure funnel, tensions from 0 to 400 cm of water were measured and the pressure plate was used for measuring tensions up to 12

bars. Undisturbed soil samples with 7.6 cm diameter and 7.6 cm depth were taken from the field using an undisturbed soil sampler.

Table 4.3. Laboratory measurements of saturated hydraulic conductivity (vertical)

Layer	Number of core samples	Mean of ln sat. hyd. conductivity cm/hr	Standard deviation of ln sat. hyd. conductivity cm/hr
1	14	-0.5886	1.0815
2	15	-0.1367	0.7206
3	26	1.2009	0.9189
4	15	0.7394	2.3407

Porosity

Dry bulk density of the soil samples was determined by drying and weighing the samples. The porosity was determined from the relationship:

$$n = \frac{V_v}{V_t} = 1 - \rho_b/\rho_s \qquad (4.2)$$

where

V_v = volume of the void,

V_t = volume of the total soil sample,

ρ_b = dry bulk density, and

ρ_s = density of soil particle ($\approx$ 2.65).

Particle size, pH and organic contents were determined following standard lab procedures.

CHAPTER 5. RESULTS AND DISCUSSION

The validity of a model is tested by comparing the numerical solutions with either an analytical solution, if it is available, or observed data. In this study, the model is tested against observed data. A model is valid only if the approximate solution is satisfactorily accurate or close to the exact solution if one exists. When tested against observed data, a valid model should produce results similar to the observed data (provided that the observed data are accurate). Convergence and stability are the two terms usually associated with numerical models. Convergence is satisfied when the approximation approaches the exact solution as step sizes of the spatial and temporal discretization approach zero. A model is said to be stable if the amplification of the error is restricted or has a finite limit as the computation marches forward in time (Chung, 1985).

The model, as developed, was tested using field observations over a period of 373.5 hours starting at 10:30 a.m. on May 25, 1987 and ending at midnight on June 9, 1987. This period was chosen because there was appreciable rainfall (Fig. 5.1) and tile outflow during this period.

The Boundary Conditions

It is necessary to fix the boundary conditions before the program can be executed. The soil profile (Fig. 5.2) was divided into 72 nodes and 55 elements (Appendix B). The nodes on BC were treated as evaporation/ infiltration boundaries. The nodes on CD were treated as no flow nodes, i.e., water cannot enter or move out through this boundary.

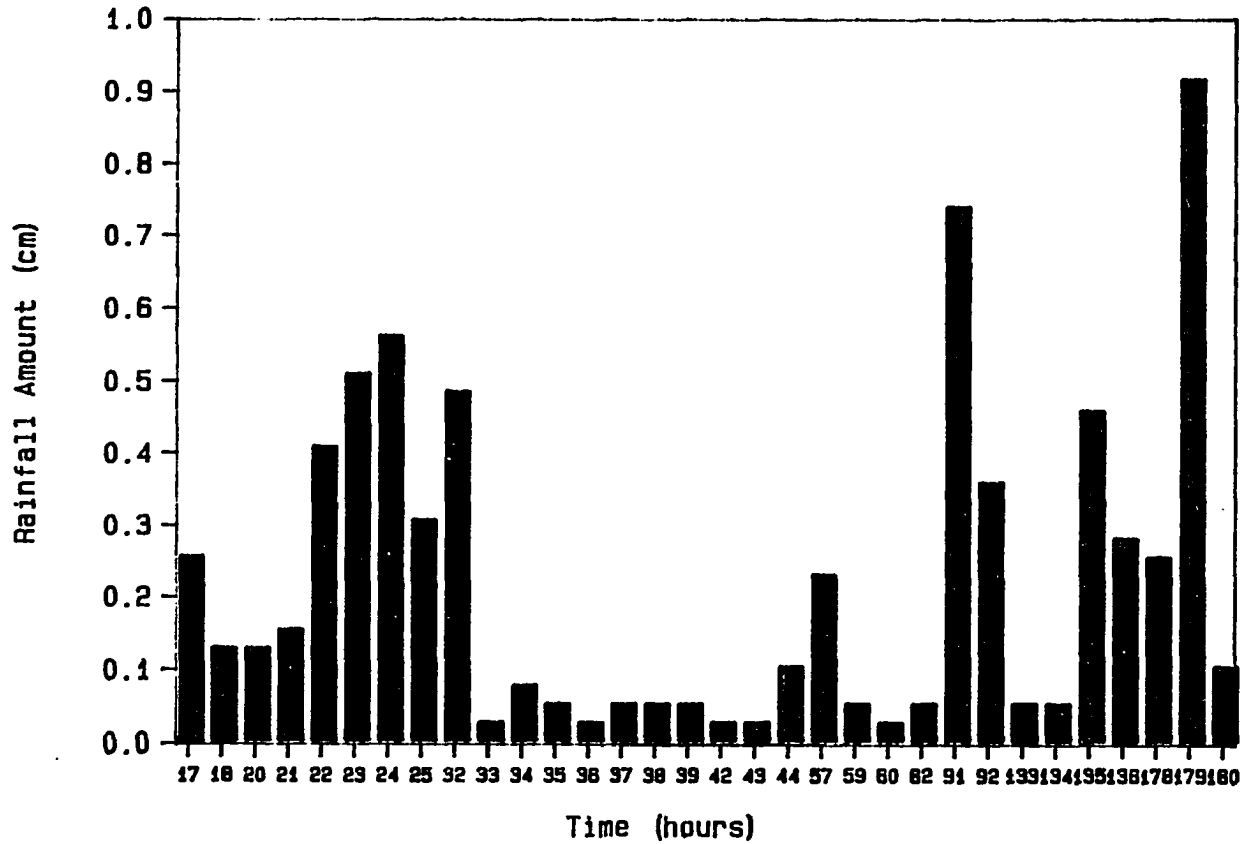

Figure 5.1. Rainfall during the simulated period

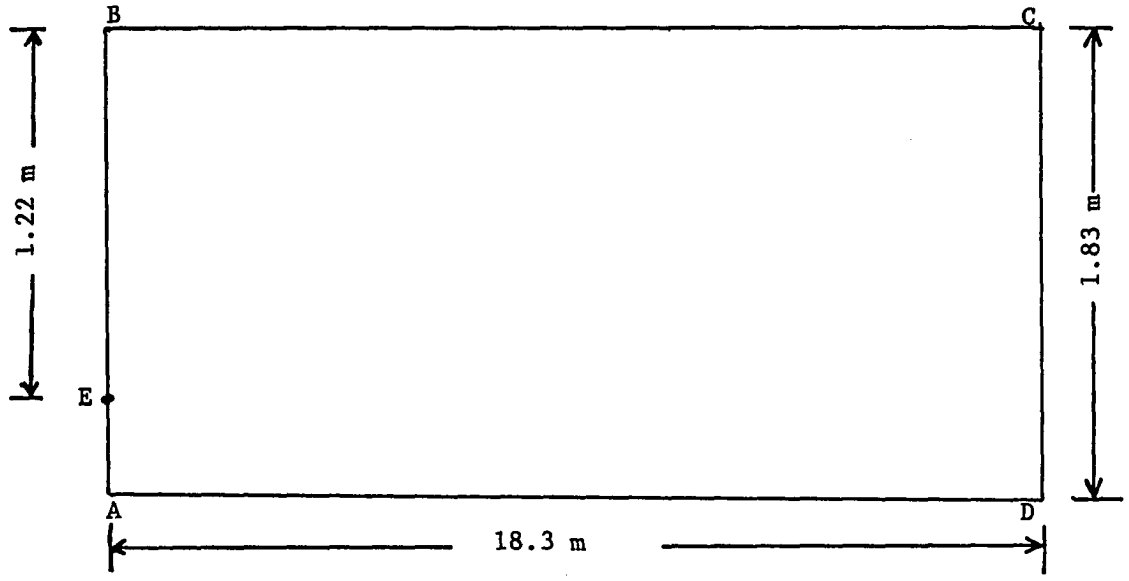

Figure 5.2. The soil profile

The nodes on AB were also treated as no flow nodes except a node at E, which was designated as a seepage node to simulate the presence of a tile at that particular point. Water can flow out of the profile through a seepage node when that node becomes saturated. To fix the boundary at face AD posed some problems. The following types of boundary conditions can be envisioned for this face:

1. Known pressure heads or constant head along the face,
2. No flow across the boundary, and/or
3. A constant flux across the boundary.

As no information was available on pressure heads at this face, the first option was discarded. The second option was unrealistic as there is no information available regarding the presence of any impermeable layer at this depth. The third option was used and a constant downward flux of 5.1

cm/year was used. This value is a standard value used for central Iowa by engineers and soil scientists based on an average water balance analysis.

A Discussion on Input Data

Results obtained from a model can be only as good as the input data. Thus, before using any model, it is imperative that the modeler acquire a good knowledge about the accuracy of the data, how they were obtained, and the sensitivity of the model outputs on input data. For this particular model, the following discussion on input data will be helpful in the analysis of model performance.

1. The saturated hydraulic conductivity (vertical) values were measured in the laboratory instead of in the field and a small number of samples were used (Table 4.4). The laboratory values also did not show that the log saturated hydraulic conductivity values are normally distributed. This particular assumption is the basis for utilizing the Monte Carlo method in this research.
2. No measurements of horizontal saturated hydraulic conductivity were made. A ratio of 5:1 (horizontal saturated hydraulic conductivity to vertical saturated hydraulic conductivity) was used for the different simulations done in this study (in simulation 5, the ratio is 2:1). Rizvi (1987) did field investigations on the top 60.0 cm of this particular plot. He found the ratio of horizontal to vertical hydraulic conductivity to be in the range between 3 and 8.
3. Relative hydraulic conductivities were not measured but were estimated using van Genuchten's equations (equations 3.21 and 3.22).

4. Potential evapotranspiration was calculated using Shaw's empirical equations.
5. The soil profile was divided into four layers based on field observations. If there were more data available to divide the profile into higher numbers of layers, the heterogeneity of the soil physical properties in the profile would have been better approximated.
6. No soil samples could be taken for the depth between 121.9 cm and 182.9 cm from the surface because of limited field equipment. Thus, no soil physical properties could be measured and estimates of the parameters were used.
7. In any numerical model, the smaller the spatial and temporal step sizes generally the better are the result. But smaller step sizes mean higher computer costs. The temporal step sizes used in this study were 0.1 to 1.0 hour during rainfall events and 0.1 to 4.0 hours during evaporation events. Spatial step sizes are given in Appendix B.
8. The number of Monte Carlo runs were also kept to a minimum for economic reasons. The number of Monte Carlo runs within a simulation varied from 20 to 30 runs.

The Simulations

Six simulations were done. Table 5.1 provides information on input variables from these six simulations. The results from these simulations are presented in Tables 5.2, 5.3, 5.4, and 5.5 and in Figures 5.3, 5.4, 5.5, 5.6, 5.7, and 5.8. The simulations were based on the following:

Table 5.1. Values of input variables used in the simulation

	Simulation 1	Simulation 2
Number of Monte Carlo runs	20	20
Ratio of horizontal to vertical saturated hydraulic conductivity	5:1	5:1
Mean of ln K^s_z of layer 1 (cm/hr)	-0.5886	-0.5886
Standard deviation of ln K^s_z of layer 1	0.0815	0.5886
Mean of ln K^s_z of layer 2 (cm/hr)	-0.1367	-0.1367
Standard deviation of ln K^s_z of layer 2	0.7206	0.1367
Mean of ln K^s_z in layer 3 (cm/hr)	1.2009	1.2009
Standard deviation of ln K^s_z of layer 3	0.9189	1.2009
Mean of ln K^s_z of layer 4 (cm/hr)	0.7394	0.7394
Standard deviation of ln K^s_z of layer 4	2.3407	0.7394

Simulation 3	Simulation 4	Simulation 5	Simulation 6
20	20	20	30
5:1	5:1	2:1	5:1
-0.5886	-1.2817	-1.2817	-1.2817
0.2943	0.6409	0.6409	0.6409
-0.1367	-0.8298	-0.8298	-0.8298
0.0684	0.4149	0.4149	0.4149
1.2009	0.6005	0.6005	0.6005
0.6005	0.3003	0.3003	0.3003
0.7394	0.3697	0.3697	0.3697
0.3697	0.1849	0.1849	0.1849

Table 5.2. Predicted depth of water table from surface

Time (hrs)	Simulation 1 mean (cm)[a]	Simulation 1 s.d. (cm)	Simulation 2 mean (cm)	Simulation 2 s.d. (cm)	Simulation 3 mean (cm)	Simulation 3 s.d. (cm)
49.5	124.6	9.96	116.7	7.22	113.5	3.16
97.5	116.1	11.58	106.0	2.48	104.2	0.80
169.5	115.7	14.30	109.0	7.91	108.6	4.69
217.5	112.6	16.34	106.6	9.64	106.4	5.56
265.5	119.9	13.71	119.5	8.55	120.3	4.49
337.5	134.2	15.96	136.4	8.32	137.3	4.41

[a]Water table predictions are at 18.3 m from the tile.

Simulation 4		Simulation 5		Simulation 6		
mean (cm)	s.d. (cm)	mean (cm)	s.d. (cm)	mean (cm)	s.d. (cm)	Measured (cm)
117.2	3.85	117.1	3.81	117.1	3.25	131.4
105.0	1.40	102.7	2.45	104.9	1.17	113.4
103.9	2.52	98.2	1.25	103.9	2.12	103.3
100.9	3.26	92.7	2.14	100.9	2.74	103.3
115.4	3.76	105.8	3.20	115.6	3.17	107.6
132.0	3.85	125.3	3.79	132.2	3.24	114.9

Table 5.3. Predicted cumulative outflow through the tile

Time (hrs)	Simulation 1 mean (cm^2)	Simulation 1 s.d. (cm^2)	Simulation 2 mean (cm^2)	Simulation 2 s.d. (cm^2)	Simulation 3 mean (cm^2)	Simulation 3 s.d. (cm^2)
61.5	614.9	666.2	3901.1	311.8	340.3	160.8
109.5	1411.6	1293.7	1197.7	665.2	1138.9	347.6
157.5	1903.5	1487.2	1904.4	807.5	1890.8	444.0
204.5	2607.7	1899.4	2670.5	978.0	2684.4	538.2
253.5	2779.1	1824.6	2978.0	878.5	3027.9	471.9
301.5	2809.6	1795.2	2993.0	856.3	3032.0	465.3
349.5	2813.6	1789.5	2993.0	856.3	3032.0	465.3

Simulation 4		Simulation 5		Simulation 6		
mean (cm^2)	s.d. (cm^2)	mean (cm^2)	s.d. (cm^2)	mean (cm^2)	s.d. (cm^2)	Measured (cm^2)
180.4	83.9	123.4	56.3	180.8	70.5	59.1
799.1	186.1	536.3	124.4	802.6	156.3	434.6
1474.1	237.4	991.5	166.1	1479.4	199.3	1109.6
2185.3	293.9	1495.1	221.3	2192.2	246.8	1699.0
2631.7	241.3	1830.5	208.7	2638.5	202.6	2192.7
2655.7	214.9	1859.5	189.5	2658.8	180.4	2502.7
2655.7	214.9	1859.5	189.5	2658.8	180.4	2675.6

Table 5.4. Predicted tile outflow rate

Time (hrs)	Simulation 1 mean (cm^2/hr)[a]	Simulation 1 s.d. (cm^2/hr)	Simulation 2 mean (cm^2/hr)	Simulation 2 s.d. (cm^2/hr)	Simulation 3 mean (cm^2/hr)	Simulation 3 s.d. (cm^2/hr)
37.5	37.41	47.67	12.64	17.05	5.11	8.08
49.5	8.97	12.69	16.56	11.27	16.55	6.44
73.5	5.70	7.07	12.58	4.82	13.12	2.51
97.5	38.59	36.00	31.00	18.93	28.16	9.87
109.5	9.97	10.47	20.77	6.24	21.76	3.48
133.5	3.18	3.69	6.82	3.09	8.66	0.76
145.5	23.42	18.35	22.60	10.43	21.64	5.90
169.5	4.13	4.45	8.91	2.62	10.74	0.67
193.7	21.01	17.10	31.05	12.69	30.39	6.19
217.5	5.11	5.23	10.59	2.90	12.49	0.87
241.5	2.09	2.59	2.82	2.60	2.82	2.12
265.5	0.98	1.35	0.60	1.04	0.18	0.46
289.5	0.38	0.62	0.07	0.23	0.00	0.00

[a]Units of tile outflow are in $cm^3/hr/cm$ of tile length.

Simulation 4		Simulation 5		Simulation 6		
mean (cm^2/hr)	s.d. (cm^2/hr)	mean (cm^2/hr)	s.d. (cm^2/hr)	mean (cm^2/hr)	s.d. (cm^2/hr)	Measured (cm^2/hr)
0.00	0.00	0.00	0.00	0.00	0.00	0.00
9.28	5.48	6.37	3.63	9.54	4.61	2.18
10.67	1.59	7.07	1.03	10.76	1.34	6.13
18.19	4.91	12.30	3.40	18.16	4.13	7.27
18.73	2.10	12.46	1.34	18.89	1.77	16.12
9.97	0.55	6.64	0.25	9.97	0.47	14.08
15.71	3.25	10.96	2.58	15.68	2.73	12.26
11.50	0.16	7.95	0.24	11.53	0.14	12.26
23.60	4.16	16.95	3.34	23.70	3.50	12.26
13.73	0.36	9.82	0.27	13.76	0.31	12.26
5.57	1.45	4.61	0.49	5.54	1.22	8.85
1.05	1.27	1.30	0.80	0.84	1.11	7.27
0.03	0.12	0.06	0.19	0.02	0.10	6.13

Table 5.5. Predicted pressure heads at different nodes at time 51.5 hrs

Node	Depth from surface (cm)	Pressure Simulation 1 mean	s.d.	Simulation 2 mean	s.d.	Simulation 3 mean	s.d.
40	15.24	-95.0	13.7	-97.0	6.8	-97.8	3.2
41	30.48	-78.5	11.8	-79.5	5.7	-80.2	2.5
42	60.96	-48.1	11.5	-49.6	4.8	-49.9	2.2
43	91.44	-31.0	6.5	-25.0	3.2	-22.9	1.3
45	121.92	-2.9	8.5	4.3	5.4	7.3	1.4
52	15.24	-94.9	12.8	-96.5	5.7	-97.4	2.5
53	30.48	-78.2	11.1	-78.8	4.6	-79.5	1.7
54	60.96	-47.8	10.9	-49.8	3.7	-49.0	1.4
55	91.44	-30.5	7.11	-23.9	4.0	-21.6	2.1
57	121.92	-2.4	9.2	5.5	6.3	8.7	2.3

heads (cm)

Simulation 4		Simulation 5		Simulation 6		
mean	s.d.	mean	s.d.	mean	s.d.	Measured
-90.9	6.4	-90.7	6.2	-91.4	5.4	-71.0
-77.8	1.8	-77.5	1.5	-77.8	1.5	-63.0
-47.9	1.2	-47.6	1.0	-47.9	1.0	-55.0
-24.4	2.5	-23.7	3.0	-24.2	2.1	-35.0
5.7	2.7	6.5	3.2	6.0	2.3	-4.0
-91.6	5.9	-91.7	5.9	-92.0	5.0	-69.0
-77.8	1.5	-77.9	1.5	-77.8	1.3	-61.0
-47.8	0.9	-48.0	0.9	-47.9	0.8	-52.0
-24.1	3.0	-24.2	3.3	-23.9	2.7	-33.0
6.2	3.4	6.1	3.6	6.3	2.9	-5.0

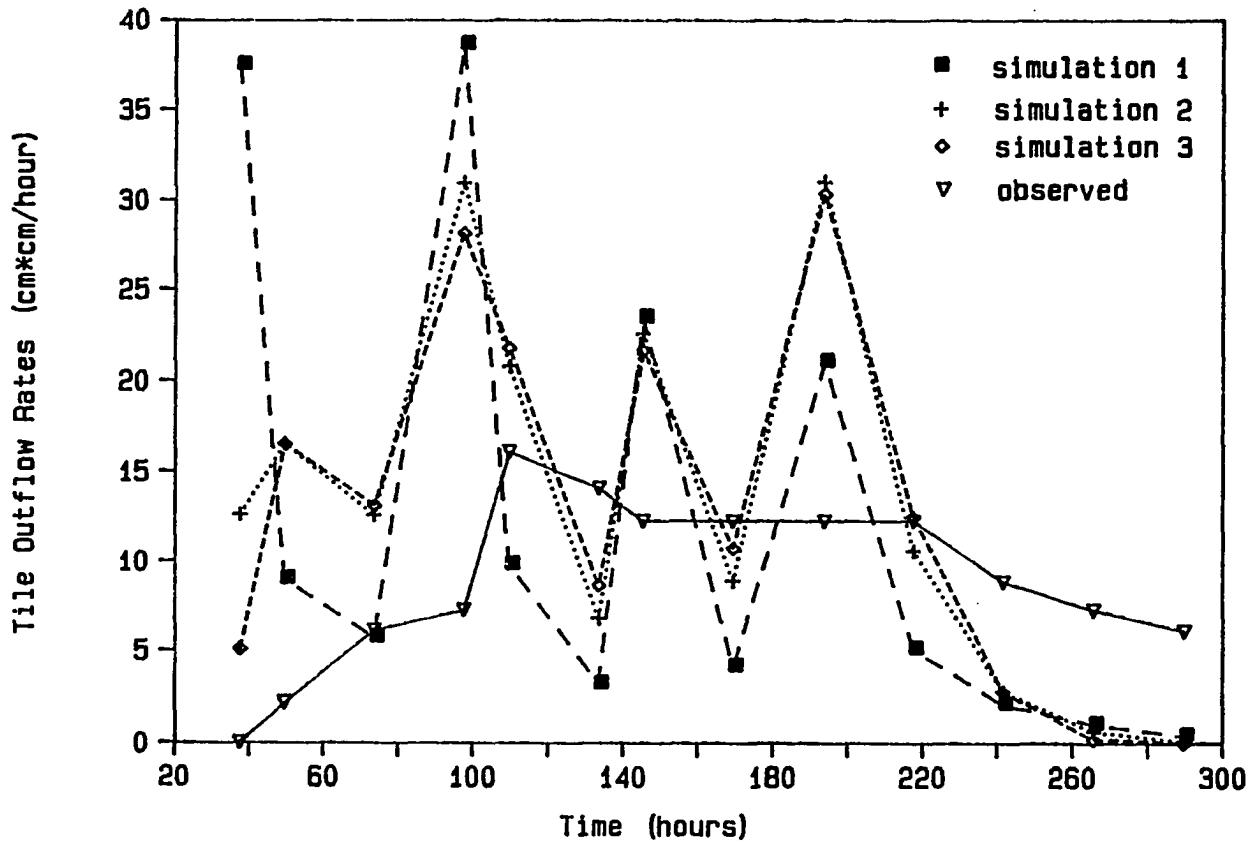

Figure 5.3. Predicted tile outflow rates by the various simulations

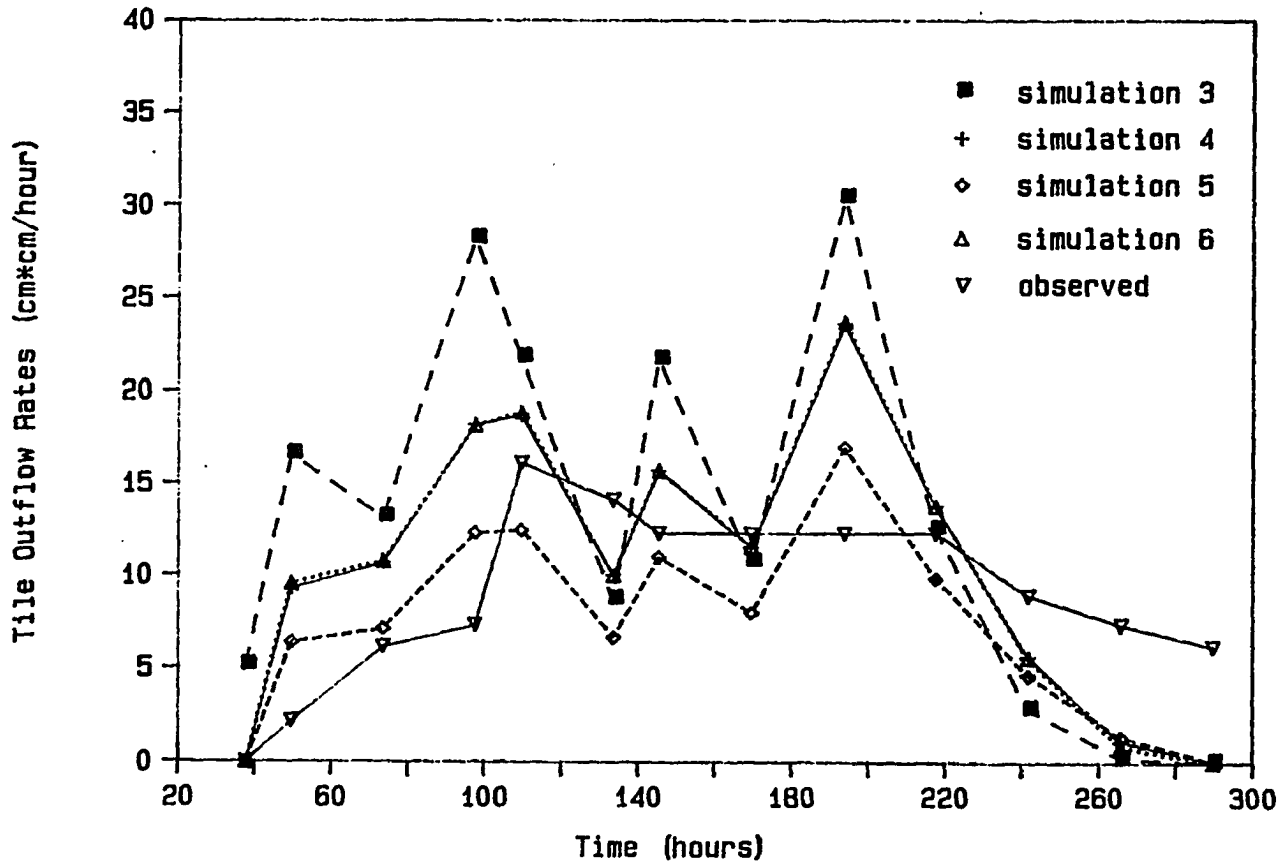

Figure 5.4. Predicted tile outflow rates by the various simulations

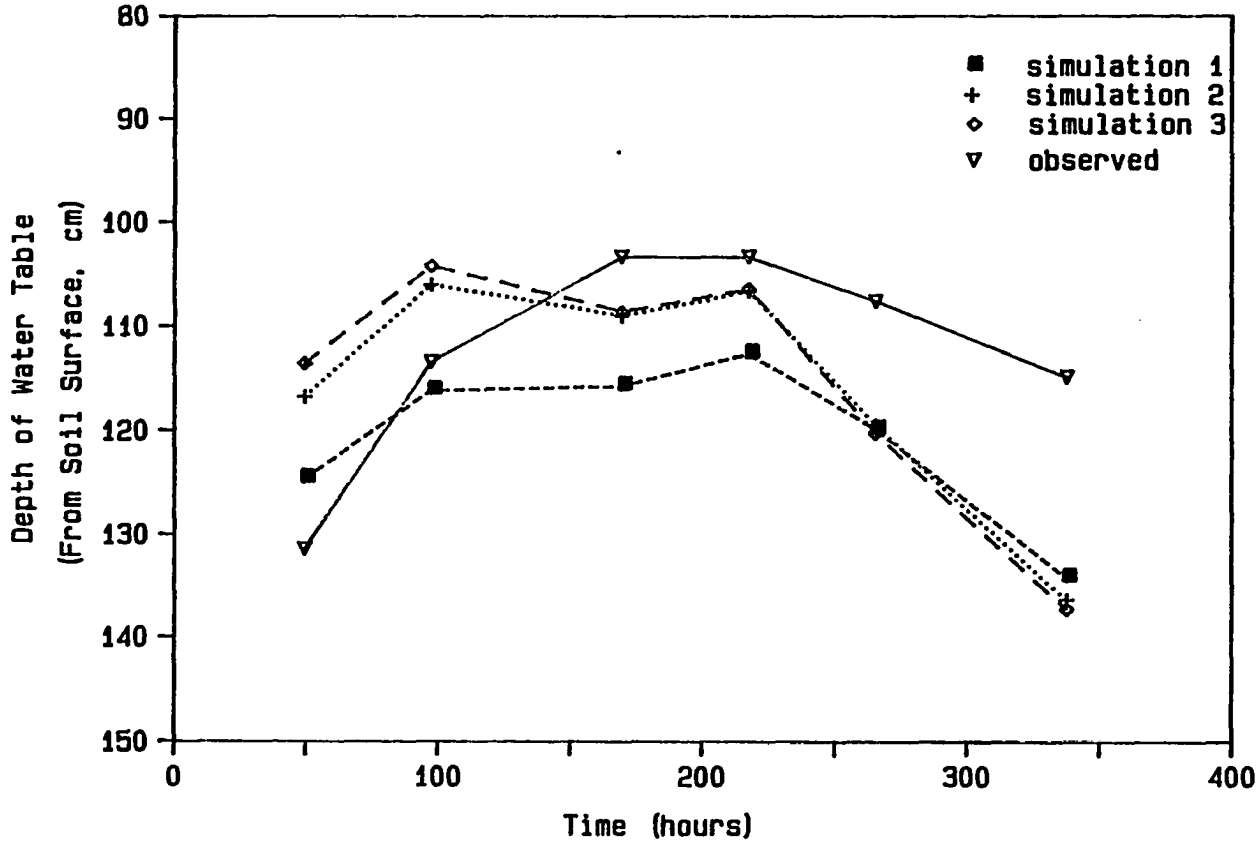

Figure 5.5. Predicted water table depths by the various simulations

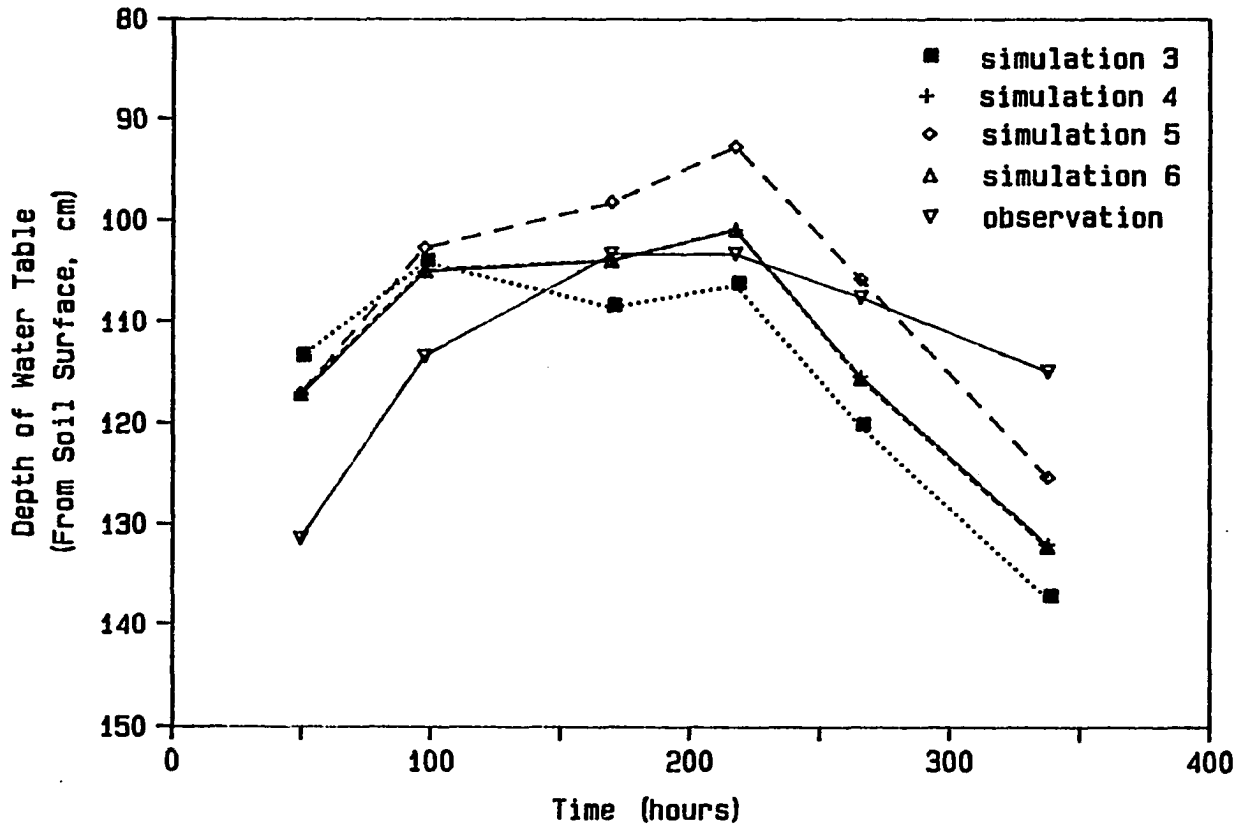

Figure 5.6. Predicted water table depths by the various simulations

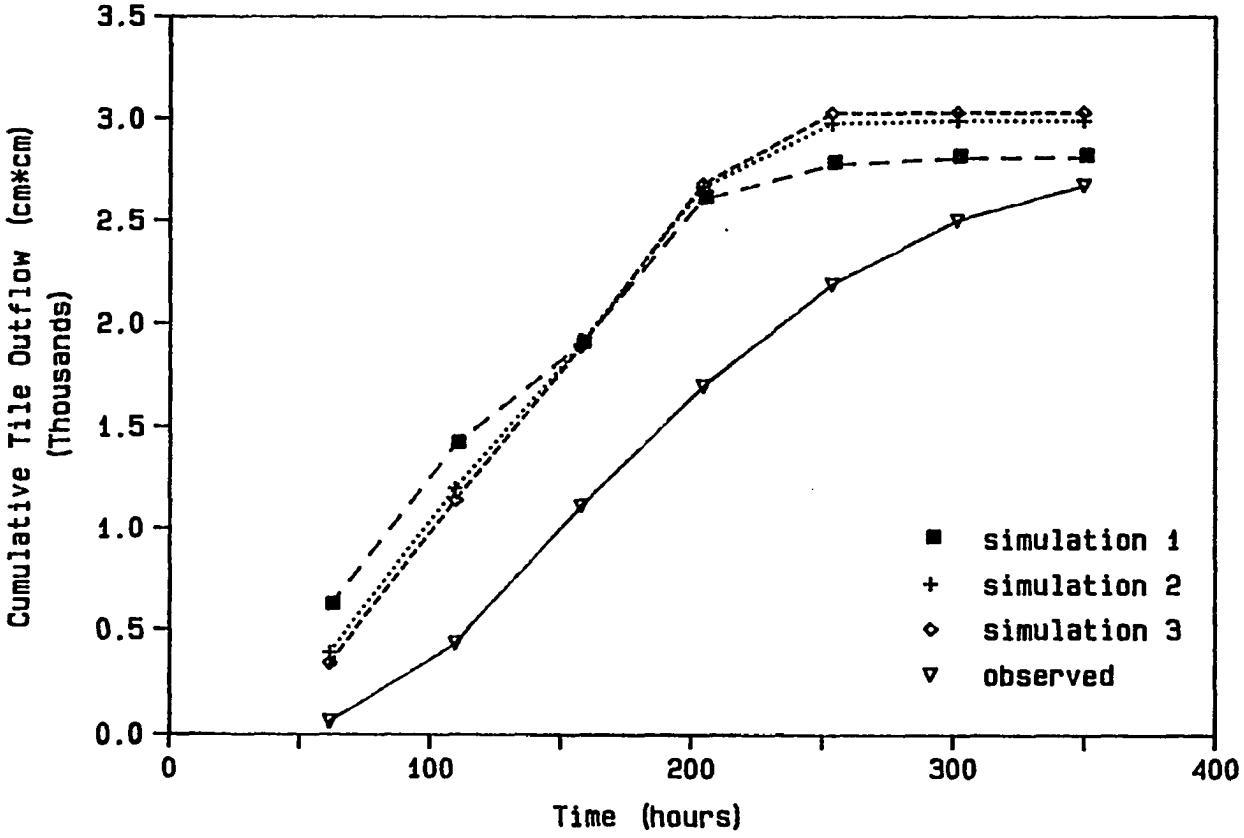

Figure 5.7. Predicted cumulative tile outflow by the various simulations

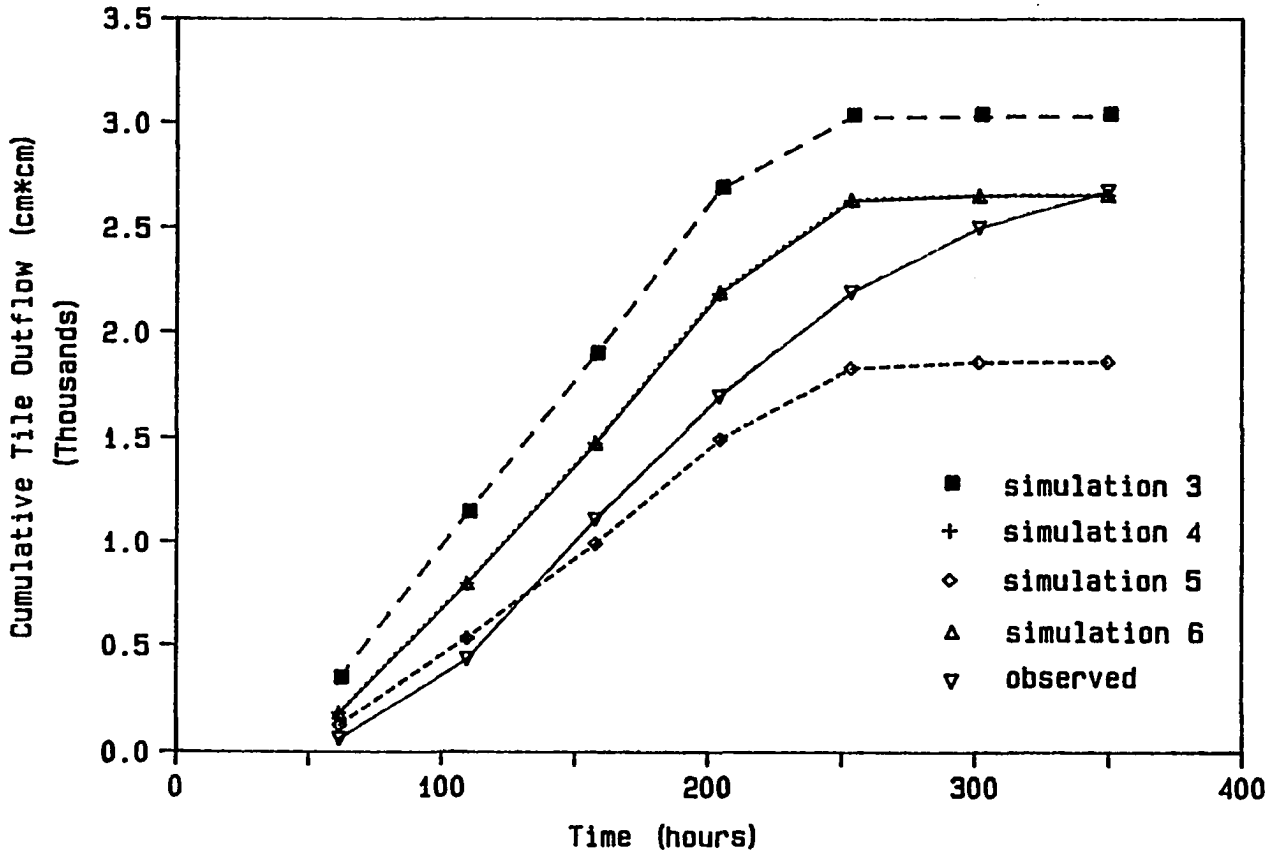

Figure 5.8. Predicted cumulative tile outflow by the various simulations

1. No plant component was considered because the plants were small and the rooting depth was probably not more than a few centimeters. The estimated potential evapotranspiration was considered as potential evaporation only.
2. Rainfall and potential evaporation data were provided on 4 or 8 hourly increments (Figure 5.1 provides information on rainfall and pan evaporation data and are given in Appendix B). Rainfall and potential evaporation intensity were assumed constant during these time periods. The reasons for using 4 or 8 hourly increments are as follows:
   a. The daily potential evapotranspiration values are divided into six 4-hour increments on the basis of information provided by Anderson (1975).
   b. The observed tile outflow rates do not show any rapid response to rainfall events.
3. The empirical Shaw's method was used for calculating potential evaporation.

Simulation 1

In this simulation, the means of laboratory values of log saturated hydraulic conductivity were used. The standard deviations of log saturated hydraulic conductivities as obtained in the laboratory for the four layers were used for generating twenty sets of saturated hydraulic conductivity (vertical) values for twenty Monte Carlo runs. The ratio of horizontal to vertical saturated hydraulic conductivity was 5:1. Analyzing the results from simulation 1, it is seen that the total amount of tile outflow is 2,813.6 cm^2 which is almost identical to the measured total outflow of

2,828.3 cm^2. The fact to note is that the model was run up to midnight of June 9, 1987 but the tile continued to flow until June 12, 1987. It is clear from the results of simulation 1 that the predicted tile outflow rates (Fig. 5.3) are much higher than observed in the periods after rainfall events. The peaks in the outflow rates occur right after rainfall events. The tile starts flowing earlier and becomes dry earlier than observed. The water table rises earlier and goes down earlier, also. The standard deviations of all the output variables are very high.

Simulation 2

Mean values of log saturated hydraulic conductivity as obtained in the laboratory were used. Standard deviations were set such that the coefficient of variations were equal to 1.0. These parameters were used to generate twenty sets of K^s_z for twenty Monte Carlo runs. The K^s_x:K^s_z ratio was 5:1. The results are similar to simulation 1 except that the standard deviations are much lower in simulation 2. The total tile outflow is 2993.0 cm^2 which is a little higher (6%) than the observed total outflow.

Simulation 3

Mean values of log K^s_z are the same as in simulations 1 and 2 but the standard deviations are set as fifty percent of mean values. The total number of Monte Carlo runs is twenty and the ratio of K^s_x:K^s_z is 5:1. The results show similar trends as in simulations 1 and 2. The tile outflow rate at 37.5 hours is much less than rates from simulations 1 and 2. The

total outflow is 3032.0 cm^2. The standard deviations of outflow variables are much less than those of simulations 1 and 2.

Simulation 4

Mean values of log K^s_z are lowered by fifty percent and standard deviations are fifty percent of mean values. There are twenty Monte Carlo runs and the ratio of K^s_x:K^s_z is 5:1. The output variables, such as tile outflow rates, are much smaller than those of simulations 1, 2 and 3. The total outflow is 2656.0 cm^2 which is about 6% less than observed outflow. The standard deviations are also much lower than those of simulations 1, 2 and 3.

Simulation 5

The only difference is the ratio of K^s_x:K^s_z is assumed to be 2:1. The total tile outflow is 1860.0 cm^2 which is about 34% less than observed total outflow. The tile outflow rates show similar trends like simulation 4 but the rates are much lower. The predicted depths of water table throughout the simulation period (which is measured at a horizontal distance of 18.3 m from the tile) are always higher than those of simulation 4.

Simulation 6

The only difference in this simulation from simulation 4 is that the total number of Monte Carlo runs is 30 instead of 20. The results are identical to simulation 4 except that the standard deviations of output

variables in simulation 6 are lower than standard deviations in simulation 4.

Sensitivity Analysis

Results obtained from the previously mentioned six simulations can be used for sensitivity analysis. The results were compared to see the:

1. relationship between the input and output standard deviations,
2. effects of input hydraulic conductivity values on output variables,
3. effect of the input ratio of horizontal to vertical hydraulic conductivity on output variables, and
4. effect of the number of Monte Carlo runs on output variables.

Effect of input standard deviations of ln K^S_z values on standard deviations of output variables

The mean values of ln K^S_z in simulation 2 and simulation 3 are the same, but the standard deviations of ln K^S_z are 50% lower in simulation 3 than in simulation 2. Tables 5.6, 5.7 and 5.8 show the effects of such differences on output variables. In all these cases, the standard deviation of output variables are much lower in simulation 3. These results show a direct relationship between input and output standard deviations. Predicted pressure heads at 51.5 hours at different nodes also show the same trend.

Effect of input mean ln K^S_z on output variables

Results from simulation 3 and simulation 4 should be compared to see the effects of input mean ln K^S_z values on output variables. The input mean ln K^S_z values in simulation 4 are about 50% lower than those of

Table 5.6. Comparison of predicted tile outflow rates of simulation 2 and simulation 3

Time	Coefficient of variation		Percent change
	Simulation 2	Simulation 3	
49.5	0.6806	0.3891	-42.83
73.5	0.3831	0.1913	-50.07
97.5	0.6106	0.3505	-42.60
109.5	0.3004	0.1599	-46.77
133.5	0.4531	0.0878	-80.62
145.5	0.4615	0.2726	-40.93
169.5	0.2941	0.0624	-78.78
193.7	0.4087	0.2037	-50.16
217.5	0.2738	0.0697	-74.56
241.5	0.9220	0.7518	-18.46

Table 5.7. Comparison of the predicted cumulative outflow through the tile of simulation 2 and simulation 3

Time	Coefficient of variation		Percent change
	Simulation 2	Simulation 3	
61.5	0.7993	0.4725	-40.89
109.5	0.5554	0.3052	-45.05
157.5	0.4240	0.2348	-44.62
204.5	0.3662	0.2005	-45.25
253.5	0.2950	0.1559	-47.15
301.5	0.2861	0.1535	-46.35

Table 5.8. Comparison of predicted water table depths of simulation 2 and simulation 3

Time	Coefficient of variation		Percent change
	Simulation 2	Simulation 3	
49.5	0.0619	0.2784	-55.00
97.5	0.2340	0.0077	-67.18
169.5	0.0726	0.0432	-40.49
217.5	0.0904	0.0522	-42.23
265.5	0.0716	0.0373	-47.84
337.5	0.0610	0.0321	-47.34

simulation 3. Input standard deviations are 50% of mean values in both the cases. Looking at Table 5.3 and Figure 5.6, it is seen that the water table rises slowly and recedes slowly in simulation 4 compared to simulation 3. The peak is higher in simulation 4 and at 337.5 hours, the water table is 5.3 cm higher in simulation 4 compared to simulation 3. The total tile outflow predicted in simulation 4 is about 88% that of simulation 3. Table 5.9 shows the changes in tile outflow rates. It shows that the peak values are considerably less in simulation 4 compared to simulation 3. Thus, it can be said that input hydraulic conductivity values have a significant effect on the predicted output variables. These all happen due to the slower movement of soil-moisture in the soil profile in simulation 4. Predicted pressure heads at 51.5 hours in Table 5.6 clearly show that, too.

Effect of input ratio of horizontal to vertical saturated hydraulic conductivity on output variables

Results from simulation 4 and simulation 5 should be compared to see the effect of input ratio of horizontal to vertical saturated hydraulic conductivity on output variables. In simulation 4, the ratio is 5:1, but in simulation 5, the ratio is 2:1. The predicted total tile outflow in simulation 5 is about 70.0% that of simulation 4. Comparing the predicted water table depths, it is seen that the peak water table depth is 8.1 cm (at 217.5 hours) higher in simulation 5 and, at 337.5 hours, it is still 6.7 cm higher in simulation 5. This is due to the fact that in the soil profile, the water moves much more slowly towards the tile in simulation 5. Hence, there is the build up of the water table. Tile outflow rates are

Table 5.9. Predicted mean tile outflow rates of simulation 3 and simulation 4

Time	Mean of tile outflow rates (cm^2/hr)		Percent change
	Simulation 3	Simulation 4	
37.5	5.11	0.00	
49.5	16.55	9.28	-43.93
73.5	13.12	10.67	-18.67
97.5	28.16	18.19	-35.40
109.5	21.76	18.73	-13.92
133.5	8.66	9.97	15.13
145.5	21.64	15.71	-27.40
169.5	10.74	11.50	7.08
193.7	30.39	23.60	-22.34
217.5	12.49	13.73	9.93
241.5	2.82	5.57	97.52

also considerably less in simulation 5 than those of simulation 4. As the total tile outflow is less in simulation 5, the soil profile as a whole is wetter at the end of the simulation period (373.5 hours) in simulation 5 in comparison with simulation 4.

Effect of the number of Monte Carlo runs on output variables

The input variables in simulation 4 and simulation 6 are the same except for the number of Monte Carlo runs in simulation 4 is 20 whereas in simulation 6 the number is 30. Comparing the output variables in Tables 5.2, 5.3, 5.4, and 5.5 it is seen that there is very little change in the mean values of output variables, but standard deviations are somewhat less in simulation 6 (Tables 5.10, 5.11, and 5.12). By increasing the number of Monte Carlo runs, it is possible to lower the standard deviations, but there will come a time when further increase in Monte Carlo runs will not produce appreciable change in standard deviations of output variables. Increasing the number of Monte Carlo runs results in higher costs in running the program.

A Discussion of the Results

Analyzing the outputs from the six simulations, it is seen that the predicted cumulative tile outflow values are close to the observed values (except for simulation 5). The model with the given saturated hydraulic conductivity values in all the simulations responds rapidly to rainfall events. Thus, tile outflow rates and water table fluctuations do not match the observed values. The tile also flows for a shorter duration than observed duration. In light of the more rapid response of the model, it

Table 5.10. Comparison of predicted tile outflow rates of simulation 4 and simulation 6

Time	Coefficient of variation		Percent change
	Simulation 4	Simulation 6	
49.5	0.5931	0.4832	-18.53
73.5	0.1490	0.1245	-16.44
97.5	0.2699	0.2274	-15.75
109.5	0.1121	0.0938	-16.32
133.5	0.0552	0.0471	-14.67
145.5	0.2069	0.1741	-15.85
169.7	0.0139	0.0121	-16.22
217.5	0.0262	0.0225	-14.12
241.5	0.2603	0.2202	-15.41

Table 5.11. Comparison of the predicted cumulative outflow through the tile of simulation 4 and simulation 6

Time	Coefficient of variation		Percent change
	Simulation 4	Simulation 6	
61.5	0.4651	0.3899	-16.16
109.5	0.2329	0.1947	-16.38
157.5	0.1610	0.1347	-16.32
204.5	0.1345	0.1126	-16.30
253.5	0.0917	0.0768	-16.26
301.5	0.0809	0.0679	-16.07

Table 5.12. Comparison of predicted water table depths of simulation 4 and simulation 6

Time	Coefficient of variation		Percent change
	Simulation 4	Simulation 6	
49.5	0.03285	0.02775	-15.52
97.5	0.01333	0.01115	-16.35
169.5	0.02425	0.02040	-15.88
217.5	0.03231	0.02716	-15.94
265.5	0.03258	0.02742	-15.84
337.5	0.02917	0.02451	-15.98

appears that the saturated hydraulic conductivity values in running the model may be higher than those which actually exist in the field. It is also uncertain that the relative hydraulic conductivity values estimated by van Genuchten's method truly represent the field situations. The same can be said about the soil moisture characteristics curve for the four layers obtained in the laboratory. Uncertainties also exist in the assumption of constant downward flux in the bottom boundary, the ratio of saturated horizontal hydraulic conductivity to saturated vertical hydraulic conductivity, in the estimation of potential evaporation by Shaw's methods (Equation 2.21) and estimation of surface runoff by the Soil Conservation Service (SCS) method (Equation 3.17).

Considering the above mentioned factors, we can say the following things about the model:

1. The model is able to predict tile outflow rate, pressure heads in the soil profile, water content in the unsaturated zone and other variables as outlined in the objectives of this research.
2. The model will work well only if very good input data are provided.
3. Using laboratory data for modeling field situations should be done with caution.
4. Empirical and theoretical methods of calculating potential evapotranspiration, surface runoff, and unsaturated hydraulic conductivity should be used with great caution.
5. Horizontal saturated hydraulic conductivity values play an important role in the predicted output variables.

Conclusions

Conclusions based on the present study are listed as follows:

1. The finite element method can be successfully applied to model two dimensional saturated-unsaturated soil-moisture flow based on the continuity theory.
2. The Monte Carlo method can be applied for taking into consideration the stochastic nature of saturated hydraulic conductivity of the layered soil profile.
3. The mean and standard deviation of saturated hydraulic conductivity and the ratio of horizontal to vertical saturated hydraulic conductivity, have significant effects on output variables such as water table depths, tile outflow rates, total tile outflow, pressure head, etc.
4. Laboratory values of soil physical properties should be used with great caution in modeling field situations. Greater emphasis and effort should be placed in determining soil physical properties in the field.
5. Horizontal hydraulic conductivity plays an important role in determining tile outflow rate and total amount.

ACKNOWLEDGMENTS

I express my sincere gratitude to my major professor, Dr. T. Al Austin, for his guidance and supervision throughout my research work. Grateful appreciation is due to the members of my graduate committee, Dr. R. A. Lohnes of the Civil and Construction Engineering Department, Drs. C. E. Anderson and J. L. Baker of the Agricultural Engineering Department, and Dr. R. Horton of the Agronomy Department, for their guidance. I am also thankful to Dr. R. Allen for getting me involved in this research project.

I also deeply appreciate the financial support received from the Iowa State Water Resources Research Institute and the Department of Civil and Construction Engineering at Iowa State University.

I am indebted to all my family members and close personal friends for their encouragement, patience, and help during the course of the study.

Last, but not least, my grateful thanks to my dearest wife, Lucy, for her sacrifices, patience, understanding, and constant encouragement. And to my daughter, Roxanne, I dedicate this work.

REFERENCES

Anderson, C. E. 1975. "A water balance model for agricultural watersheds on deep loess soils." Ph.D. Thesis. Kansas State University, Manhattan, Kansas.

Anderson, C. E., Johnson, H. P., and Powers, W. L. 1978. "A water-balance model for deep loess soils." Trans. ASAE 21(2):314-320.

Aslyng, H. C. 1963. "Soil physics terminology." International Society of Soil Science Bulletin 23:7.

Bakr, A. A., Gelhar, L. W., Gutjahr, A. L., and MacMillan, J. R. 1978. "Stochastic analysis of spatial variability in subsurface flows: 1. Comparison of one- and three-dimensional flows." Water Resources Research 14(2):263-271.

Bear, J. 1972. Dynamics of Fluids in Porous Media. American Elsevier, Inc., New York, N.Y.

Bear, J., and Verruijt, A. 1987. Modeling Groundwater Flow and Pollution. D. Reidel Publishing Company, Boston.

Bennion, D. W., and Griffiths, J. C. 1966. "A stochastic model for predicting variations in reservoir rock properties." Soc. of Petrol. Engineers (March 1966), pp. 9-16.

Bennion, D. W., and Hope, A. C. A. 1974. "Mathematical modeling of reservoir rock properties." Journal of Canadian Petroleum Technology 13(2):46-55.

Bianchi, W. C., and Haskell, E. E., Jr. 1966. "Air in the vadose zone as it affects water movements beneath a recharge basin." Water Resources Research 2:315-322.

Brooks, R. H., and Corey, A. T. 1964. "Hydraulic properties of porous media." Colorado State University Hydrology Paper No. 3.

Bulnes, A. C. 1946. "An application of statistical methods to core analysis data of dolomitic limestone." Trans. AIME 165:223-240.

Campbell, G. S. 1974. "A sample method for determining unsaturated conductivity from moisture retention data." Soil Science 117(6):311-314.

Chung, Sang-Ok. 1985. "Stochastic modeling of water movement in the saturated-unsaturated zone." Ph.D. Thesis. Iowa State University, Ames, Iowa.

DeBoer, D. W. 1969. "Flood hydrology of watersheds with depressional storage." Ph.D. Thesis, Iowa State University, Ames, Iowa.

Feddes, R. A. 1971. "Water, heat, and crop growth." Ph.D. Thesis. State Agricultural University, Wageningen, The Netherlands.

Feddes, R. A., Bresler, E., and Neuman, S. P. 1974. "Field test of a modified numerical model for water uptake by root systems." Water Resources Research, 10(6): 1199-1206.

Feddes, R. A., Kowalik, P. J., and Zaradny, H. 1978. Simulation of Field Water Use and Crop Yield. John Wiley and Sons, New York, N.Y.

Fleming, G. 1975. Computer Simulation Techniques in Hydrology. Elsevier, New York, N.Y.

Freeze, R. A. 1975. "A stochastic-conceptual analysis of one-dimensional groundwater flow in nonuniform homogeneous media." Water Resources Research 11(5):725-741.

Freeze, R. A., and Cherry, J. A. 1979. Groundwater. Prentice-Hall, Inc., Englewood Cliffs, New Jersey.

Fritschen, L. J., and Shaw, R. H. 1961. "Transpiration and evapotranspiration of corn as related to meteorological factors." Agronomy Journal 53:71-74.

Fujioka, Y., and Kitamura, T. 1964. "Approximate solution of a vertical drainage problem." Journal of Geophysical Research 69(24):5249-5255.

Gardner, W. R. 1964. "Relation of root distribution to water uptake and availability." Agronomy Journal 56:35-41.

Gelhar, L. W. 1976. "Effects of hydraulic conductivity variations on groundwater flows." pp. 409-429 in Proceedings 2nd International IAHR Symposium in Stochastic Hydraulics. Lund Institute of Technology, Lund, Sweden.

Green, D. W., Dabiri, H., Weinaug, C. F., and Prill, R. 1970. "Numerical modeling of unsaturated groundwater flow and comparison of the model to a field experiment." Water Resources Research 6:862-874.

Green, W. H., and Ampt, G. A. 1911. "Studies on soil physics: I. Flow of air and water through soils." Journal of Agricultural Science 4:1-24.

Hammersley, J. M., and Handscomb, D. C. 1964. Monte Carlo Methods. Methuen and Co., LTD., London.

Harrold, L. L., Peters, D. B., Dreibelbis, F. R., and McGuinness, J. L. 1959. "Transpiration evaluation of corn grown on a plastic covered lysimeter." Proc. Soil Sci. Soc. Amer. 23:174-178.

Hillel, D. 1982. Introduction to Soil Physics. Academic Press, New York, N.Y.

Holtan, H. N., England, C. B., and Shanholtz, V. Q. 1967. "Concepts in hydrologic soil grouping." Trans. ASAE 10(3):407-410.

Jensen, M. E., Wright, J. L., and Pratt, B. J. 1971. "Estimating soil moisture depletion from climate, crop, and soil data." Trans. ASAE 14(5):954-959.

Kanwar, R. S. 1981. "Hydrologic simulation of nitrate losses with tile drainage water." Ph.D. Thesis. Iowa State University, Ames, Iowa.

Lapidus, L., and Pinder, G. F. 1982. Numerical Solution of Partial Differential Equations in Science and Engineering. John Wiley and Sons, New York.

Law, J. 1944. "A statistical approach to the interstitial heterogeneity of sand reservoirs." Trans. AIME 155:202-222.

McMillan, W. D. 1966. "Theoretical analysis of groundwater basin operation." Technical Report 6-25. Hydraulic Lab., University of California, Berkeley.

McWhorter, D. B. 1971. "Infiltration affected by flow of air." Colorado State University Hydrology Paper 49. Fort Collins, Colorado.

Milly, P. C. D., and Eagleson, P. S. 1980. "The coupled transport of water and heat in a vertical soil column under atmospheric excitation." Report No. 258. Department of Civil Engineering, Massachusetts Institute of Technology, Cambridge, Massachusetts.

Mockus, V. 1972. "Estimation of direct runoff from storm rainfall." In National Engineering Handbook, Section 4, Hydrology. U.S. Soil Conservation Service, Washington, D.C.

Molz, F. G., and Remson, I. 1970. "Extraction term models of soil moisture use by transpiring plants." Water Resources Research 6(5):1346-1356.

Mualem, Y. 1976. "A new model for predicting the hydraulic conductivity of unsaturated porous media." Water Resources Research 13(4):773-780.

Neuman, S. P., and Davis, L. A. 1983. Documentation and User's Guide: Unsat2 - Variably Saturated Flow Model. U.S. Nuclear Regulatory Commission, Washington, D.C.

Neuman, S. P., Feddes, R. A., and Bresler, E. 1974. "Finite element simulation of flow in saturated-unsaturated soils considering water uptake by plants." Israel Institute of Technology, Hydrodynamics & Hydraulic Engineering Lab., Haifa, Israel.

Nimah, M. N., and Hanks, R. J. 1973. "Model for estimating soil, water, plant, and atmosphere interactions: 1. Description and sensitivity." Soil Sci. Soc. Amer. Proc. 37:522-527.

Nielsen, D. R., Biggar, J. W., and Erh, K. T. 1973. "Spatial variability of field-measured soil-water properties." Hilgardia 42(7):215-259.

Peters, D. B., and Russell, M. B. 1959. "Relative water losses by evaporation and transpiration in field corn." Soil Sci. Soc. Proc. 23:170-173.

Philip, J. R., and de Vries, D. A. 1957. "Moisture movement in porous materials under temperature gradients." Transactions of American Geophysical Union 38:222-228.

Prickett, T. A. 1975. "Modeling techniques for groundwater evaluation." Adv. Hydrosci. 10:1-143.

Remson, I., Hornberger, G. M., and Molz, F. J. 1971. Numerical Methods in Subsurface Hydrology with an Introduction to the Finite Element Method. Wiley Interscience, New York.

Richtmyer, R. D., and Morton, K. W. 1967. Difference Methods for Initial Value Problems. 2nd ed. Wiley Interscience, New York.

Ritchie, J. T. 1972. "Model for predicting evaporation from a row crop with incomplete cover." Water Resources Research 8(5):1204-1213.

Rizvi, S. H. A. 1987. "Tillage and wheel traffic effect on hydraulic conductivity." M.S. Thesis. Iowa State University, Ames, Iowa.

Rubinstein, R. Y. 1981. Simulation and the Monte Carlo Method. John Wiley & Sons, New York.

Saxton, K. E. 1972. "Watershed evapotranspiration by the combination method." Ph.D. Thesis. Iowa State University Library, Ames, Iowa.

Saxton, K. E., Johnson, H. P., and Shaw, R. H. 1974. "Modeling evapo-transpiration and soil moisture." Trans. ASAE 17(4): 673-677.

Segerlind, L. J. 1984. Applied Finite Element Analysis. John Wiley and Sons, New York.

Shahghasemi, E. 1980. "Simulation modeling of erosion processes on small agricultural watersheds." Ph.D. Thesis. Iowa State University, Ames, Iowa.

Shahvar, Z. 1981. "Simulation of water requirements for irrigation of corn on three soils in Iowa." Ph.D. Thesis. Iowa State University, Ames, Iowa.

Shaw, R. H. 1963. "Estimation of soil moisture under corn." Iowa Agric. Home Econ. Exp. Stn. Res. Bull. 520.

Skaggs, R. W. 1978. "A water management model for shallow water table soils." Report No. 134. Water Resources Research Institute, North Carolina State University, Raleigh, N.C.

Smith, J. L. 1978. "A stochastic analysis of steady-state groundwater flow in a bounded domain." Ph.D. Thesis. University of British Columbia, Canada.

Smith, L., and Freeze, R. A. 1979a. "Stochastic analysis of steady state groundwater flow in a bounded domain: 1. One-dimensional simulations." Water Resources Research 15(3):521-528.

Smith, L., and Freeze, R. A. 1979b. "Stochastic analysis of steady state groundwater flow in a bounded domain: 2. Two-dimensional simulations." Water Resources Research 15(6):1543-1559.

Smith, R. E., and Hebbert, R. H. B. 1979. "A Monte Carlo analysis of the hydrologic effects of spatial variability of infiltration." Water Resources Research 15(2):419-429.

Sobol, I. M. 1974. The Monte Carlo Method. The University of Chicago Press, Chicago.

Tang, D. H., and Pinder, G. F. 1977. "Simulation of groundwater flow and mass transport under uncertainty." Advances in Water Resources 1(1):25-30.

Tanner, C. B. 1960. "Energy balance approach to evapotranspiration from crops." Soil Sci. Soc. Am. Proc. 24:1-9.

Todd, D. K. 1980. Groundwater Hydrology. John Wiley and Sons, New York.

van Genuchten, M. T. 1980. "A closed equation for predicting the hydraulic conductivity of unsaturated soils." Soil Science Society of America Journal 44:892-898.

Wang, H. F., and Anderson, M. P. 1982. Introduction to Groundwater Modeling. W. H. Freeman and Company, San Francisco, California.

Warren, J. E., Skiba, F. F., and Price, H. S. 1961. "An evaluation of the significance of permeability measurement." J. Petrol. Technol. 13:739-744.

Warrick, A. W., Mullen, G. J., and Nielsen, D. R. 1977. "Prediction of soil water flux based upon field-measured soil water properties." Soil Science Society of America Journal 41:14-19.

Wells, R. D. 1978. "Moisture distribution in processed oil shale profiles affected by atmospheric evaporation and storms." M.S. Thesis. University of Idaho, Moscow, Idaho.

Willardson, L. S. and Hurst, R. L. 1965. "Sample size estimates in permeability studies." Journal of Irrigation and Drainage Division, ASCE 91(IR1):1-9.

Wilson, L. G., and Luthin, J. N. 1963. "Effect of air flow ahead of the wetting front on infiltration." Soil Science 96:136-143.

Youngs, E. G., and Peck, A. J. 1964. "Moisture profile development and air compression during water uptake by bounded porous bodies: 1. Theoretical introduction." Soil Science 98:280-294.

APPENDIX A: LOCAL COORDINATE FUNCTIONS

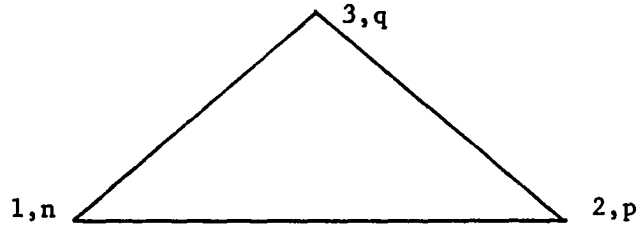

Figure A.1. Triangular element

Referring to Figure A.1, the relationship between local coordinate functions (N_1, N_2, N_3) and global Cartesian coordinates in a vertical cross-section described by the coordinates X and Z is given by:

$$\begin{bmatrix} 1 \\ X \\ Z \end{bmatrix} = \begin{bmatrix} 1 & 1 & 1 \\ X^1 & X^2 & X^3 \\ Z^1 & Z^2 & Z^3 \end{bmatrix} \begin{bmatrix} N^e{}_1 \\ N^e{}_2 \\ N^e{}_3 \end{bmatrix} \tag{A.1}$$

The inverse of Equation A.1 is:

$$\begin{bmatrix} N^e{}_1 \\ N^e{}_2 \\ N^e{}_3 \end{bmatrix} = \frac{1}{2\Delta} \begin{bmatrix} a_1 & b_1 & c_1 \\ a_2 & b_2 & c_2 \\ a_3 & b_3 & c_3 \end{bmatrix} \begin{bmatrix} 1 \\ X \\ Z \end{bmatrix} \tag{A.2}$$

Where the area of a triangle, Δ, is given by:

$$\Delta = \begin{vmatrix} 1 & X^1 & Z^1 \\ 1 & X^2 & Z^2 \\ 1 & X^3 & Z^3 \end{vmatrix} = b_1 c_2 - c_1 b_2 \tag{A.3}$$

and

$$
\begin{array}{lll}
a_1 = x^2 z^3 - x^3 z^2 & b_1 = z^2 - z^3 & c_1 = x^3 - x^2 \\
a_2 = x^3 z^1 - x^1 z^3 & b_2 = z^3 - z^1 & c_2 = x^1 - x^3 \\
a_3 = x^1 z^2 - x^2 z^1 & b_3 = z^1 - z^2 & c_3 = x^2 - x^1
\end{array}
\qquad (A.4)
$$

APPENDIX B: DATA

1. Rainfall

Date	Time (hrs) From	To	Amount (cm)
05/26/87	3.00	4.00	.254
	4:00	5:00	.127
	6:00	7:00	.127
	7:00	8:00	.152
	8:00	9:00	.406
	9:00	10:00	.508
	10:00	11:00	.559
	11:00	12:00	.305
	18:00	19:00	.483
	19:00	20:00	.025
	20:00	21:00	.076
	21:00	22:00	.051
	22:00	23:00	.025
	23:00	24:00	.051
05/27/87	0:00	1:00	.051
	1:00	2:00	.051
	4:00	5:00	.025
	5:00	6:00	.025
	6:00	7:00	.102
	19:00	20:00	.229
	21:00	22:00	.051
	22:00	23:00	.025
05/28/87	0:00	1:00	.051
05/29/87	5:00	6:00	.737
	6:00	7:00	.356
05/30/87	23:00	24:00	.051
05/31/87	0:00	1:00	.051
	1:00	2:00	.457
	2:00	3:00	.279
06/01/87	21:00	22:00	.254
	22:00	23:00	.914
	23:00	24:00	.102
06/10/87	13:00	14:00	.152

2. Pan evaporation (cm)

Date	Pan evaporation	Date	Pan evaporation
05/25/87	0.254	06/01/87	0.838
05/26/87	0.508	06/02/87	0.965
05/27/87	0.787	06/03/87	0.889
05/28/87	0.508	06/04/87	0.787
05/29/87	0.610	06/05/87	1.092
05/30/87	0.737	06/06/87	1.194
05/31/87	0.813	06/07/87	1.295
		06/08/87	1.143
		06/09/87	0.991

3. Soil water retention data (drying curve)

Pressure head (cm)	Water content (Θ_v)			
	Layer 1	Layer 2	Layer 3	Layer 4
-10.0	.4259	.473	.4657	.4316
-30.0	.4199	.4629	.4541	.4141
-55.0	.4116	.4489	.4388	.3984
-88.0	.4034	.4352	.409	.3789
-110.0	.3946	.4201	.402	.3632
-150.0	.3825	.4025	.396	.3466
-190.0	.3722	.3874	.390	.333
-325.0	.3444	.3499	.375	.3023
-1000.0	.2767	.2724	.235	.2408
-12000.0	.1539	.1614	.168	.141

4. Relative hydraulic conductivity, $k^r(\theta)$ [has been estimated using equations (3.21) and (3.22)]

Layer 1		Layer 2	
Water content θ_v	$k^r(\theta)$	Water content θ_v	$k^r(\theta)$
.1498	5.867×10^{-7}	.1545	0.856×10^{-7}
.182	4.615×10^{-6}	.1847	1.248×10^{-6}
.2141	2.161×10^{-5}	.2148	9.543×10^{-6}
.2462	1.179×10^{-4}	.2450	4.947×10^{-5}
.2783	4.518×10^{-4}	.2752	1.986×10^{-4}
.3104	1.55×10^{-3}	.0353	6.678×10^{-4}
.3425	5.006×10^{-3}	.3355	1.986×10^{-3}
.3746	1.626×10^{-2}	.3657	5.442×10^{-3}
.4067	6.291×10^{-2}	.3959	1.531×10^{-2}
.4282	1.0	.4260	3.814×10^{-2}
		.4562	1.186×10^{-1}
		.4763	1.0

Layer 3		Layer 4	
Water content θ_v	$k^r(\theta)$	Water content θ_v	$k^r(\theta)$
.1659	2.107×10^{-7}	.1381	4.92×10^{-8}
.198	1.204×10^{-5}	.1703	6.001×10^{-7}
.2295	1.3×10^{-4}	.2026	4.651×10^{-6}
.2613	7.166×10^{-4}	.2349	2.650×10^{-5}
.3010	3.727×10^{-3}	.2671	1.215×10^{-4}

4. (continued)

Layer 3		Layer 4	
Water content θ_v	$k^r(\theta)$	Water content θ_v	$k^r(\theta)$
.3328	1.116×10^{-2}	.2994	4.774×10^{-4}
.3646	2.992×10^{-2}	.3317	1.694×10^{-3}
.3884	6.06×10^{-2}	.3639	5.731×10^{-3}
.4202	1.6×10^{-1}	.3962	2.016×10^{-2}
.4480	5.186×10^{-1}	.4285	1.015×10^{-1}
.4697	1	.4392	1

5. Nodal point data

Node	X coordinate (cm)	Z coordinate (cm)	Type of node
1	0.0	182.88	evap/infilt
2	0.0	177.80	internal
3	0.0	172.74	internal
4	0.0	167.64	internal
5	0.0	152.64	internal
6	0.0	121.92	internal
7	0.0	91.44	internal
8	0.0	66.04	internal
9	0.0	60.96	seepage
10	0.0	50.96	internal
11	0.0	40.96	internal

5. (continued)

Node	X coordinate (cm)	Z coordinate (cm)	Type of node
12	0.0	0.0	constant flux
13	100.0	182.88	evap/infilt
14	100.0	177.80	internal
15	100.0	172.74	internal
16	100.0	167.64	internal
17	100.0	152.40	internal
18	100.0	121.92	internal
19	100.0	91.44	internal
20	100.0	66.04	internal
21	100.0	60.96	internal
22	100.0	50.96	internal
23	100.0	40.96	internal
24	100.0	0.0	constant flux
25	300.0	182.88	evap/infilt
26	300.0	177.80	internal
27	300.0	172.74	internal
28	300.0	167.64	internal
29	300.0	152.40	internal
30	300.0	121.92	internal
31	300.0	91.44	internal
32	300.0	66.04	internal
33	300.0	60.96	internal
34	300.0	50.96	internal
35	300.0	40.96	internal
36	300.0	0.0	internal
37	609.6	182.88	evap/infilt
38	609.6	177.80	internal
39	609.6	172.74	internal
40	609.6	167.64	internal
41	609.6	152.40	internal

5. (continued)

Node	X coordinate (cm)	Z coordinate (cm)	Type of node
42	609.6	121.92	internal
43	609.6	91.44	internal
44	609.6	66.04	internal
45	609.6	60.96	internal
46	609.6	50.96	internal
47	609.6	40.96	internal
48	609.6	0.0	constant flux
49	1219.2	182.88	evap/infilt
50	1219.2	177.80	internal
51	1219.2	172.74	internal
52	1219.2	167.64	internal
53	1219.2	152.40	internal
54	1219.2	121.92	internal
55	1219.2	91.44	internal
56	1219.2	91.44	internal
56	1219.2	66.04	internal
57	1219.2	60.96	internal
58	1219.2	50.96	internal
59	1219.2	40.96	internal
60	1219.2	0.0	constant flux
61	1828.8	182.88	evap/infilt
62	1828.8	177.80	internal
63	1828.8	172.74	internal
64	1828.8	167.64	internal
65	1828.8	152.40	internal
66	1828.8	121.92	internal
67	1828.8	91.44	internal
68	1828.8	66.04	internal
69	1828.8	60.96	internal
70	1828.8	50.96	internal

5. (continued)

Node	X coordinate (cm)	Z coordinate (cm)	Type of node
71	1828.8	40.96	internal
72	1828.8	0.0	constant flux

6. Observed pressure heads (cm)

Date	Depths (cm)	Location 1 (x=0.0 m)	Location 2 (x=6.1 m)	Location 3 (x=12.2 m)	Location 4 (x=18.3 m)
05/25/87	15.0	-139.0	-121.0	-136.0	-127.0
10:30 hrs	30.0	-106.0	-105.0	-107.0	-108.0
	61.0	-75.0	-77.0	-77.0	-78.0
	91.0	-45.0	-41.0	-46.0	-45.0
	122.0	-15.0	-12.0	-16.0	-13.0
05/27/87	15.0	-72.0	-71.0	-69.0	-73.0
13:30 hrs	30.0	-60.0	-63.0	-61.0	-63.0
	61.0	-50.0	-55.0	-52.0	-49.0
	91.0	-26.0	-35.0	-33.0	-35.0
	122.0	3.0	04.0	-5.0	-6.0
06/01/87	15.0	-89.0	-90.0	-87.0	-82.0
13:30 hrs	30.0	-75.0	-73.0	-69.0	-65.0
	61.0	-52.0	-49.0	-41.0	-40.0
	91.0	-27.0	-22.0	-16.0	-13.0
	122.0	2.0	8.0	16.0	20.0
06/03/87	15.0	-107.0	-103.0	-100.0	-99.0
16:00 hrs	30.0	-73.0	-69.0	-74.0	-69.0
	61.0	-45.0	-42.0	-46.0	-39.0
	91.0	-26.0	-19.0	-20.0	-14.0
	122.0	-2.0	10.0	15.0	22.0

7. Observed tile outflow rates

Date	Time (hrs)	Tile outflow rates (cfs)	The equivalent tile outflow rates for the modeled portion (cm^2/hr)
05/27/87	0.00	0.0	0.0
	6:45	0.000120	0.545[a]
	12:00	0.000525	2.38
	24:00	0.001350	6.13
05/28/87	12:00	0.001225	5.56
	24:00	0.001600	7.27
05/29/87	12:00	0.001475	6.70
	24:00	0.003550	16.12
05/30/87	12:00	0.003550	16.12
	24:00	0.003100	14.08
05/31/87	12:00	0.002700	12.26
	24:00	0.002700	12.26
06/01/87	12:00	0.002700	12.26
	24:00	0.002700	12.26
06/02/87	12:00	0.002700	12.26
	24:00	0.002700	12.26
06/03/87	12:00	0.002700	12.26
	24:00	0.002300	10.45
06/04/87	12:00	0.001950	8.86
	24:00	0.001600	7.27
06/05/87	12:00	0.001600	7.27
	24:00	0.001350	6.13
06/06/87	12:00	0.001350	6.13
	24:00	0.001350	6.13
06/07/87	12:00	0.000880	4.00
	24:00	0.000880	4.00

7. (Continued)

Date	Time (hrs)	Tile outflow rates (cfs)	The equivalent tile outflow rates for the modeled portion (cm^2/hr)
06/08/87	12:00	0.000570	2.59
	24:00	0.000570	2.59
06/09/87	12:00	0.000570	2.59
	24:00	0.000480	2.18
06/10/87	12:00	0.000400	1.82
	24;00	0.000400	1.82
06/11/87	12:00	0.000320	1.45
	24:00	0.000240	1.09
06/12/87	12:00	0.000240	1.09
	24:00	0.000000	0.0

[a]The tile serves an area 368.0 ft long and 120.0 ft wide. The tile is situated in the middle. The modeled portion is 60.0 ft (18.3 m) wide. Thus, 0.000120 cfs is equivalent to $\frac{.000120 \times 60.0 \times (12.0 \times 2.54)^2 \times 60 \times 60}{368.0 \times 120.0} = 0.545\ cm^2/hr$ for the modeled portion.

8. Locations of tensiometers and observation wells

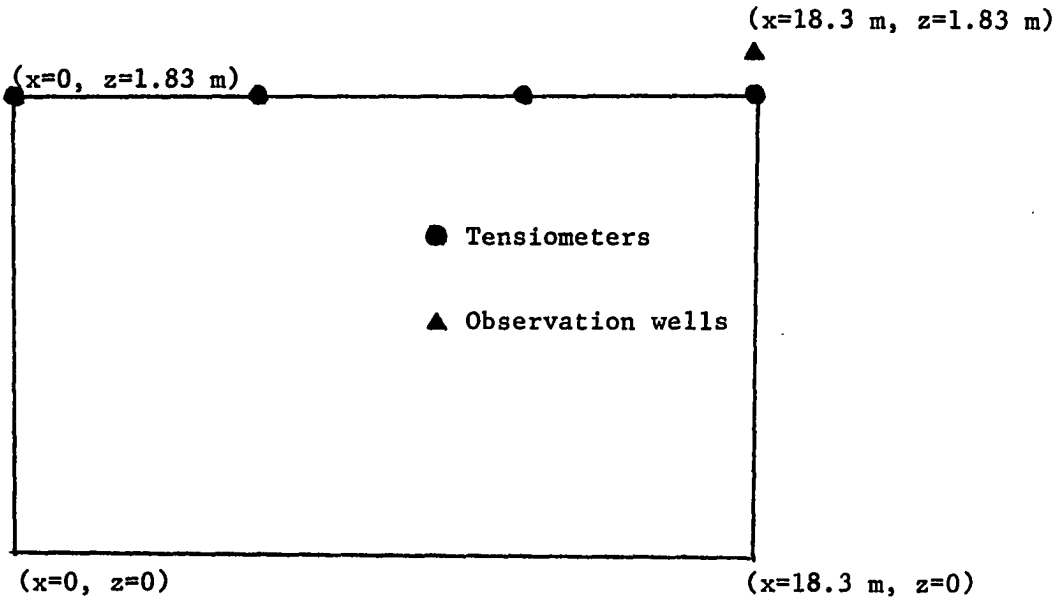

Figure B.1. Locations of tensiometers and observation wells